



RESEARCH ARTICLE

10.1029/2021JD034585

Key Points:

- Coupled Model Intercomparison Project Phase 5 (CMIP5) rainfall biases over Kenya are associated with the representation of the Indian Ocean Walker Circulation
- Models with historical rainfall biases continue to be wet/dry in future projections, which are associated with Indian Ocean Walker Circulation (IOWC) trends
- CMIP5 rainfall projections could be usefully constrained by applying IOWC metrics

Correspondence to:

J. A. King,
james.king@sheffield.ac.uk

Citation:

King, J. A., & Washington, R. (2021). Future changes in the Indian Ocean Walker Circulation and links to Kenyan rainfall. *Journal of Geophysical Research: Atmospheres*, 126, e2021JD034585. <https://doi.org/10.1029/2021JD034585>

Received 14 JAN 2021

Accepted 10 AUG 2021

Author Contributions:

Conceptualization: James A. King, Richard Washington

Formal analysis: James A. King

Investigation: James A. King

Methodology: James A. King, Richard Washington

Project Administration: Richard Washington

Resources: Richard Washington

Supervision: Richard Washington

Visualization: James A. King

Writing – original draft: James A. King

Writing – review & editing: James A. King, Richard Washington

Future Changes in the Indian Ocean Walker Circulation and Links to Kenyan Rainfall

James A. King^{1,2}  and Richard Washington¹ 

¹School of Geography and the Environment, University of Oxford, Oxford, UK, ²Leverhulme Centre for Climate Change Mitigation, University of Sheffield, Sheffield, UK

Abstract East Africa is vulnerable to hydroclimatic variability and change, and therefore reliable projections of future rainfall are important for climate change adaptation planning. However, the region's climate is affected by complex multi-scalar processes and poorly represented in climate models, leading to uncertainty surrounding rainfall change. The importance of circulation features in controlling long-term rainfall variability provides an opportunity to constrain projections. We use a process-based climate model evaluation methodology to demonstrate links between Coupled Model Intercomparison Project Phase 5 (CMIP5) rainfall biases over Kenya and circulation biases in the Indian Ocean Walker Circulation (IOWC). During both the long and short rains, models with wet biases in historical runs continue to be wet in future. Wet future projections are associated with enhanced easterly winds over the equatorial Indian Ocean, as well as decreasing vertical velocity over Kenya and increasing vertical velocity over the Maritime Continent. We demonstrate that models with a simulated IOWC which is close to reanalysis in historical runs project different changes to Kenyan rainfall than those which do not. In particular, the projected rainfall increase during the long rains is confined to a single month (April) in these models. We call for a renewed focus on the Walker Circulation as a way to constrain uncertain rainfall projections elsewhere in the tropics.

Plain Language Summary East Africa relies on agriculture to support its population and economy. Therefore, it is important to have reliable projections of how rainfall may change in future as a result of climate change. However, current projections of rainfall are uncertain because climate models (which are used to make projections) are not able to simulate important features of the regional climate. We find that models that produce too much or too little rainfall over Kenya in the present climate continue to do so in future. These wet/dry conditions in future projections are linked to model simulations of processes linked to the Indian Ocean Walker Circulation (IOWC). If we separate out projections by only choosing models which can simulate the IOWC well, we get different rainfall projections than in models which do not simulate it well. This has implications for which projections are more reliable, which is important because models disagree on future rainfall trends.

1. Introduction

East Africa is highly vulnerable to the impacts of climate change and variability, owing to reliance on agriculture and hydroelectricity generation (Borgomeo et al., 2018). The agricultural sector, which employs a majority of the working population in Kenya, Somalia, and Ethiopia (Salami et al., 2010), is largely rain-fed; both subsistence farming and production of crops intended for export (such as coffee) are deemed to be at risk from the impacts of climate change (Jaramillo et al., 2011). Rising temperatures may result in an expansion of the transmission range of malaria in the region (Onyango et al., 2016), while the development potential of small-scale hydroelectricity generation is also dependent on the reliability of future rainfall (Kaunda et al., 2012). Links have been drawn between droughts, migration, and conflict in the region in both modern times (Thalheimer & Webersik, 2020) and in pre-colonial history, with reconstructions of past rainfall variability coinciding with oral histories recounting political unrest and food shortages (Verschuren et al., 2000). Reliable projections of climate change, especially hydrological change, are therefore of great importance for future adaptation planning.

East Africa has experienced a series of severe droughts in the last few decades, for example, in 1983–1984 and 2010–2011 (Lyon, 2014), and in 2015 (Philip et al., 2018). Drought conditions have prevailed in the

© 2021. The Authors.

This is an open access article under the terms of the [Creative Commons Attribution](https://creativecommons.org/licenses/by/4.0/) License, which permits use, distribution and reproduction in any medium, provided the original work is properly cited.

region since around 2008 (Nicholson, 2017), with a significant decline in March–April–May (MAM) rainfall observed in multiple datasets (Maidment et al., 2015; Rowell et al., 2015). Indeed, the decline in MAM rainfall is the most significant trend in the region's observational record, exceeding one standard deviation of the mean trend taken over a 35 year period between 1901 and 2013 (Hoell et al., 2017). This is particularly significant because the MAM 'long rains' are the more important of the two rainy seasons found across much of the region; both in terms of amount of rainfall, and importance for agriculture (Nicholson, 2017). Importantly, the drying trend can be attributed to a shorter long rains season, with rainfall starting later and finishing earlier from the 1980s onwards (Wainwright et al., 2019). OND ('short rains') rainfall trends are more spatially heterogeneous, with a weak increase in seasonal rainfall owing to strong interannual variability arising from teleconnections to the El Niño Southern Oscillation (Hoell & Funk, 2014; Nicholson, 2015), the Indian Ocean Dipole and associated overturning (King et al., 2020; Mutai et al., 2012), and the Madden-Julian Oscillation (Berhane & Zaitchik, 2014; Zaitchik, 2017).

Global climate models participating in Coupled Model Intercomparison Project Phase 5 (CMIP5; Taylor et al., 2012) have important systematic biases in East African rainfall seasonality (Tierney et al., 2015; Yang et al., 2015). Models overestimate rainfall during OND by up to 50% and underestimate it during MAM by a similar amount with the result that the short rains are the primary rainy season (Tierney et al., 2015). The rainfall range across the CMIP5 ensemble over East Africa (the difference between the wettest and driest models) is greater than the magnitude of the observed monthly mean rainfall in all months except April (Tierney et al., 2015).

Since the CMIP5 historical climatology exhibits large biases, projections of future East African rainfall change made using these models are uncertain. For the bimodal rainfall region, Rowell et al. (2015) found that the CMIP5 ensemble mean under the RCP8.5 scenario showed increasing rainfall during the long rains up to 2100, in direct contrast to the observed drying trend; a problem termed the "East African Climate Paradox." Despite the increasingly wet long rains, the majority of the projected rainfall increases in CMIP5 models take place during the short rains, in opposition to recent observations of little trend in this season (Endris et al., 2018; Tierney et al., 2015).

The uncertainty in future East African rainfall has been argued to be due to the unresolved nature of the relationship between dynamic and thermodynamic drivers of precipitation change; specifically, the extent to which humidity increases (following the Clausius–Clapeyron relation) are canceled out by changes to the atmospheric circulation as a result of warming (Chadwick et al., 2013; Fereday et al., 2020). The nature of tropical precipitation changes are argued to be determined by shifts in spatial patterns of zones of convergence and divergence as a result of these circulation changes (Cook et al., 2020; Pfahl et al., 2017), and the primary contributor to uncertainty in model projections of East African rainfall in both rainy seasons is varying simulations of regional circulation dynamics (Rowell & Chadwick, 2018). In this study, we focus on the dynamical changes associated with the zonal Indian Ocean Walker Circulation (IOWC) as a means of understanding projections of East African rainfall. We focus here on Kenya for several reasons: the country is relatively well instrumented although has experienced a decline in reporting stations since the 1980s (Funk et al., 2015). Kenya lies at the center of the zone of bimodal rainfall in equatorial East Africa (Dunning et al., 2016) and thus experiences more spatially homogeneous rainfall seasonality than other countries in the region (Diro et al., 2010). Finally, annual rainfall in Kenya is strongly correlated with rainfall elsewhere in the bimodal region ($r = 0.77$ – 0.93 , 1922–2012; Nicholson, 2017) and therefore Kenyan rainfall can be seen as representative of the wider situation in the region on multidecadal timescales.

The IOWC, and the zonal SST pattern known as the Indian Ocean Dipole (IOD) which can perturb the IOWC when active, are important influences on the hydroclimate of East Africa (Black, 2005; Nicholson, 2017). The IOD links East Africa to wider tropical interannual variability via non-stationary teleconnections to the El Niño Southern Oscillation (ENSO; MacLeod et al., 2020; Nicholson, 2015). The climatological overturning cell features ascent over the Maritime Continent and descent over East Africa from September to March (Zhao & Cook, 2021), which is a contributor to the relative aridity of Kenya despite its location on the equator (King et al., 2020; Nicholson, 2017). Statistical and dynamic relationships between Indian Ocean ascent and descent and rainfall over East Africa are well established during the East African rainy seasons (Behera et al., 2005; Black, 2005; King et al., 2020; Liebmann et al., 2014, 2017; Vigaud et al., 2017). The IOWC is also important for understanding intraseasonal rainfall. The vertical velocity fields over the Indian Ocean

associated with the IOWC are modulated on synoptic timescales by the Madden-Julian Oscillation (MJO) (Vellinga & Milton, 2018; Zaitchik, 2017), which can act to suppress rainfall during the short rains by enhancing the strength of the overturning Walker Circulation (Berhane & Zaitchik, 2014). Nicholson (2015) found that the zonal cell in the Indian Ocean has exerted a stronger influence on the short rains since the early 1960s. There is a strong correlation between low-level equatorial zonal winds over the Indian Ocean and East African rainfall during the short rains (Mutai et al., 2012). During the long rains, low-level zonal winds over the Congo Basin and Gulf of Guinea are also strongly correlated with East African rainfall, implying a link to the broader tropical Walker Circulation (Walker et al., 2020). The ability of CMIP5 models to simulate the Walker Circulation is therefore key to providing reliable projections of future East African rainfall (Giannini et al., 2018; Nicholson, 2017), especially given that projected short rains wetting occurs in response to a weakening of the simulated IOWC (Endris et al., 2018; Kociuba & Power, 2015; Tierney et al., 2015). Climate models show a number of limitations in this area. For example, the projected tropics-wide Walker Circulation weakening is in opposition to recent observed strengthening trends (Kociuba & Power, 2015; L'Heureux et al., 2013), meaning that representation of the circulation is a major source of uncertainty in model projections across the tropics (Giannini et al., 2018; Tierney et al., 2015). CMIP5 models have SST biases which predispose them to a positive IOD state (Cai & Cowan, 2013), resulting in increased OND rainfall over East Africa in historical mode (Black, 2005; Tierney et al., 2015). Hirons and Turner (2018) found that the wet biases in CMIP5 models during the short rains were connected to erroneous zonal winds over the equatorial Indian Ocean, whereby some models simulated easterly winds rather than the observed westerlies. This resulted in enhanced moisture advection into East Africa from the central Indian Ocean, and enhanced upwelling in the eastern Indian Ocean which further enhanced the positive IOD condition (Hirons & Turner, 2018). Since these zonal winds form part of the solenoidal structure of the IOWC (Nicholson, 2017), this indicates an important limitation in the models' simulation of East African rainfall. King et al. (2020) demonstrated that CMIP5 models' rainfall biases over Kenya can be dynamically linked to their representation of the Walker Circulation, with dry (wet) biases linked to descending (ascending) biases over East Africa. Creese, Washington, and Jones (2019), and Creese, Washington, and Munday (2019) found a weakening of the zonal overturning circulation over the Congo Basin in CMIP5 projections, which is projected to become a more important influence on East African rainfall in future (Giannini et al., 2018).

Given the complex multi-scale nature of the factors affecting East African rainfall, and the uncertainty surrounding future projections, a process-based model assessment methodology is one way to assess which projections are the most plausible (James et al., 2018; Rowell et al., 2016), as well as to guide future work using regional climate modeling (RCM) studies with GCM boundary conditions (McSweeney et al., 2015). This is particularly necessary when the signal in the CMIP5 ensemble mean may not be physically plausible, as Rowell et al. (2015) suggest; this is also the case elsewhere in tropical Africa (Creese & Washington, 2016; Washington et al., 2013). Progress has been made by determining the key variables and processes which may determine the plausibility of simulated East African rainfall (Creese & Washington, 2016; Dyer et al., 2020; Dyer & Washington, 2020; McSweeney et al., 2015). Building on recent work demonstrating a link between the IOWC and CMIP5 historical rainfall biases (King et al., 2020), we investigate the relationship between CMIP5 model projections of future East African rainfall and model dynamics linked to the IOWC. Focusing on the well-instrumented country of Kenya, we address the following research questions:

1. What are the projected changes in rainfall over Kenya in CMIP5 models up to 2100?
2. What are the projected changes in omega and zonal wind associated with the IOWC?
3. Do future projections reflect historical model biases?

The rest of the paper is organized as follows. Section 2 describes the datasets used in the study. Section 3.1 shows projected changes in East African rainfall and in dynamic fields associated with the IOWC. Section 3.2 uncovers the links between rainfall and IOWC projections, as well as between historical biases and future changes in the CMIP5 ensemble. Section 3.3 puts forward projections with a composite approach based on the plausibility of models' representations of East African climate. Section 4 discusses the findings and their implications, and Section 5 concludes the paper.

2. Data

2.1. Observations and Reanalysis

Rainfall data were obtained from version 2 of the Climate Hazards Group Infrared Precipitation with Stations data set (CHIRPSv2.0; Funk et al., 2015). This data set combines gauge observations with satellite rainfall estimates derived from infrared observations of cold cloud duration, and has been extensively validated over East Africa (Gebrechorkos et al., 2018; Kimani et al., 2017). Reanalysis data from version 2 of the Modern Era Retrospective Analysis for Research and Applications (MERRA-2; Gelaro et al., 2017) were used. While we acknowledge that reanalysis products differ in their representation of climate dynamics over tropical Africa, as a result of sparse observations (James et al., 2018; Maidment et al., 2015), MERRA-2 has performed well when validated against radiosonde observations of tropospheric winds in this region (Hua et al., 2019). While we do not consider the differences in large-scale dynamics between different reanalyses to be large enough to affect our results, given the much larger differences between CMIP5 models, we use MERRA-2 because of its strong performance in the assessment of Hua et al. (2019).

2.2. CMIP5 Models

An ensemble of 25 CMIP5 models was selected (Table 1) based on the availability of vertical velocity, zonal wind, and precipitation fields for 1975–2005 (historical) and 2020–2100 (RCP8.5). We use the RCP8.5 scenario because it is the closest to observed changes in radiative forcing due to anthropogenic activity (Sanford et al., 2014), and to elicit a clear change signal in models that would reveal the dynamics involved in future rainfall projections. The first ensemble member for each model was used (R111P1), since for a number of models this was the only one available for key fields. Since the amount of uncertainty in climate projections due to initial model conditions is relatively small for decadal projections, we do not believe our results would change significantly if different ensemble members were used. Where composites were generated, model data were interpolated onto a common $1^\circ \times 1^\circ$ grid using nearest-neighbor regridding.

3. Results

3.1. Projections

3.1.1. Projected Changes in East African Rainfall

We begin by analyzing the projected changes in Kenyan rainfall up to the end of the 21st century in the RCP8.5 scenario. Following Nicholson's (2017) work which shows that the different dynamics seen in each rainy season month limit the explanatory power of analyses which aggregate the months into seasonal totals (see also Dyer & Washington, 2021), we plot results for each month separately.

For the long rains months of March, April, and May, we find substantial variation between the models in the CMIP5 ensemble on both the sign and the magnitude of the rainfall trends despite the ensemble mean indicating a statistically significant increasing rainfall trend during this season over the period 2020–2100 (Table 2). During the long rains, fewer than half of the models project any statistically significant changes in rainfall. In March, 10 models (40%) project statistically significant rainfall increases over Kenya, with 1 model (EC-EARTH) showing a statistically significant decrease. Seven models (28%) project significant rainfall increases in April, with significant decreases in FIO-ESM. Seven models (28%) project significant wetting in May, with significant drying in 3 models (CMCC-CM, MIROC5, and MPI-ESM-LR). The ensemble mean precipitation trends are small relative to the trends seen in individual models. The ensemble mean trends in March and April are very similar (0.063 and 0.064 mm day^{−1} decade^{−1}), and in May the trend is much smaller (0.023 mm day^{−1} decade^{−1}). The models with the strongest wetting trends in each month project rainfall trends which are an order of magnitude greater.

Table 2 indicates that CMIP5 rainfall slopes under RCP8.5 are in closer agreement for the short rains months of November and December compared to October, but that there is still a great degree of variation between the individual models. The ensemble mean precipitation trends are again all significant and positive; the

Table 1
CMIP5 Models Used in This Study

Model name	Modeling group
ACCESS1-3	Commonwealth Scientific and Industrial Research Organisation and Bureau of Meteorology (Australia).
BCC-CSM1-1-M	Beijing Climate Center, China Meteorological Administration.
BNU-ESM	College of Global Change and Earth System Science, Beijing Normal University.
CanESM2	Canadian Center for Modeling and Analysis.
CCSM4	National Center for Atmospheric Research (USA).
CESM1-CAM5	National Science Foundation, Department of Energy, National Center for Atmospheric Research (USA).
CMCC-CM	Centro Euro-Mediterraneo per I Cambiamenti Climatici (Italy).
CNRM-CM5	Center National de Recherches Météorologiques (France).
CSIRO-Mk3-6-0	Commonwealth Scientific and Industrial Research Organisation in collaboration with the Queensland Climate Change Center of Excellence (Australia).
EC-EARTH	EC-EARTH consortium (Europe).
FGOALS-g2	LASG, Institute of Atmospheric Physics, Chinese Academy of Sciences; and CESS, Tsinghua University.
FIO-ESM	The First Institute of Oceanography, SOA (China).
GFDL-CM3	Geophysical Fluid Dynamics Laboratory (USA).
GISS-E2-R	Goddard Institute for Space Studies (USA).
HadGEM2-AO	Met Office Hadley Center (UK).
INMCM4	Institute for Numerical Mathematics (Russia).
IPSL-CM5A-LR	L'Institut Pierre-Simon Laplace (France).
IPSL-CM5A-MR	L'Institut Pierre-Simon Laplace (France).
IPSL-CM5B-LR	L'Institut Pierre-Simon Laplace (France).
MIROC5	National Institute for Environmental Studies (Japan), Atmosphere and Ocean Research Institute (University of Tokyo), Japan Agency for Marine-Earth Science and Technology.
MIROC-ESM-CHEM	National Institute for Environmental Studies (Japan), Atmosphere and Ocean Research Institute (University of Tokyo), Japan Agency for Marine-Earth Science and Technology.
MPI-ESM-LR	Max Planck Institute for Meteorology (Germany).
MPI-ESM-MR	Max Planck Institute for Meteorology (Germany).
MRI-CGCM3	Meteorological Research Institute (Japan).
NorESM1-M	Norwegian Climate Center.

Note. Expansions of acronyms are available online at <http://www.ametsoc.org/PubsAcronymList>.

trends in November and December are the largest of any of the rainy season months; $0.139 \text{ mm day}^{-1} \text{ decade}^{-1}$ and $0.137 \text{ mm day}^{-1} \text{ decade}^{-1}$ respectively, compared to $0.051 \text{ mm day}^{-1} \text{ decade}^{-1}$ for October. The model biases in the rainfall annual cycle therefore continue up to 2100, with the short rains wetter than the long rains in the ensemble means, despite a few very wet models in the long rains months (notably BCC-CSM1-1-M). In October, fewer than half the models project significant rainfall trends. 10 models (40%) project significant wetting and 2 models project drying (IPSL-CM5B-LR and MPI-ESM-MR). The wetting trends are robust for November and December with a majority of models agreeing on significant rainfall increases (14 models [56%] in November, 15 models [60%] in December).

3.1.2. Projected Changes in Vertical Velocity (Omega)

Explaining the differences between the rainfall projections in different models requires consideration of the models' dynamics. The 400 hPa vertical velocity (omega) field over the equatorial Indian Ocean indicates

Table 2

Slopes of the Linear Regression of Kenyan Rainfall for Each Rainy Season Month, 2020 to 2100, Under the RCP8.5 Scenario

Model	Mar	Apr	May	Oct	Nov	Dec
ACCESS1-3	0.193	0.258	0.091	0.110	0.348	0.312
BCC-CSM1-1-M	0.097	0.190	-0.011	0.087	0.152	0.136
BNU-ESM	0.074	0.072	0.108	0.323	0.320	0.346
CanESM2	0.282	0.196	0.124	0.234	0.172	0.109
CCSM4	0.107	0.021	0.013	0.092	0.075	0.189
CESM1-CAM5	0.108	0.064	0.064	0.024	-0.022	0.164
CMCC-CM	0.041	0.051	-0.121	-0.021	0.060	0.051
CNRM-CM5	-0.012	0.055	0.057	0.031	0.134	0.082
CSIRO-Mk3-6-0	0.189	0.219	-0.029	0.000	0.127	0.176
EC-EARTH	-0.077	0.011	0.003	0.015	0.184	0.053
FGOALS-g2	0.019	0.107	0.129	-0.038	0.051	0.065
FIO-ESM	-0.023	-0.120	-0.015	0.139	0.137	0.161
GFDL-CM3	0.038	0.032	-0.022	-0.076	0.235	0.352
GISS-E2-R	0.047	0.074	-0.038	-0.066	-0.018	-0.005
HadGEM2-AO	0.050	-0.033	0.005	-0.031	0.148	0.075
INMCM4	0.023	0.031	-0.060	0.164	0.139	0.033
IPSL-CM5A-LR	0.019	0.051	0.121	0.076	0.038	-0.038
IPSL-CM5A-MR	0.118	0.175	0.191	0.094	0.277	0.184
IPSL-CM5B-LR	0.044	0.072	-0.010	-0.063	-0.005	0.128
MIROC5	0.082	-0.060	-0.097	0.087	0.059	0.002
MIROC-ESM-CHEM	-0.021	-0.019	0.068	0.028	0.002	0.162
MPI-ESM-LR	0.056	0.051	-0.090	0.063	0.207	0.224
MPI-ESM-MR	0.041	0.036	-0.053	-0.086	0.164	0.057
MRI-CGCM3	0.047	-0.009	0.178	-0.046	0.388	0.311
NorESM1-M	0.049	0.039	-0.008	0.099	0.124	0.141
Ensemble mean	0.064	0.063	0.024	0.050	0.140	0.139
# Positive	22	21	14	18	23	24
# Negative	4	5	12	8	3	2

Note. Light green (red) shading indicates significance of positive (negative) trends at $p < 0.1$ and darker green (red) shading at $p < 0.05$. Units are $\text{mm day}^{-1} \text{decade}^{-1}$.

the key ascending and descending regions of the IOWC. Figures 1 and 2 display the projected trends in IOWC ascent and descent for the remainder of the 21st century for composites of the 5 models with the strongest wetting trends and the 5 models with the weakest wetting/strongest drying trends for each rainy season month.

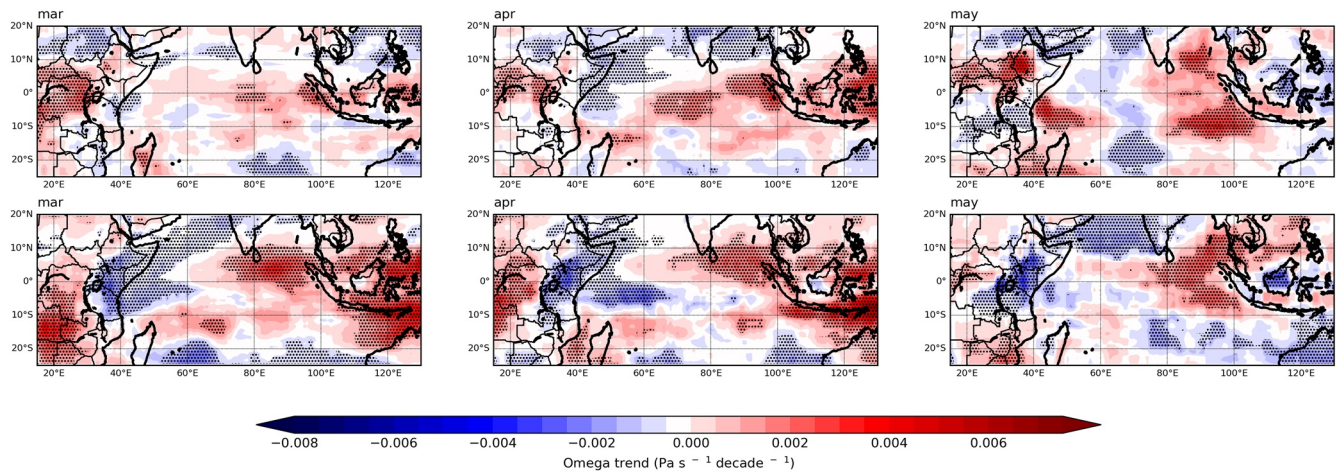


Figure 1. Linear regression trends in 400 hPa vertical velocity for March (left), April (middle), and May (right), 2020–2100, under the RCP8.5 scenario. Stippling denotes areas where $p < 0.05$. For each month, the top 5 models with strongest drying/weakest wetting (top row) and strongest wetting (bottom row) are averaged to form a composite.

In the long rains months (Figure 1), the model composites that show drying trends or weaker wetting trends over Kenya have small ($<0.002 \text{ Pa s}^{-1} \text{ decade}^{-1}$) trends toward increasing descent (positive omega) over land in East Africa. Kenya lies at the margin between a region of significant omega increase inland and omega decrease offshore in March and April. The drying/weak wetting composites also show statistically significant trends toward increasing ascent (decreasing omega) over the Maritime Continent in May, of around $-0.003 \text{ Pa s}^{-1} \text{ decade}^{-1}$. By contrast, models which produce wetting trends over Kenya exhibit strong and significant trends toward ascending air over Kenya and descending air over the Maritime Continent. This can be clearly seen in the composites forming the bottom row of Figure 1, all of which have significant areas of increasing omega over the Maritime Continent and eastern tropical Indian Ocean of $\sim 0.005 \text{ Pa s}^{-1} \text{ decade}^{-1}$. Significant omega decreases are seen over Kenya and the Greater Horn of Africa in March, April, and May, generally between -0.004 and $-0.006 \text{ Pa s}^{-1} \text{ decade}^{-1}$ over Kenya. Some individual wet models in the ensemble, for example, EC-EARTH and INMCM4, feature a strong ascending trend of $\sim 0.008 \text{ Pa s}^{-1} \text{ decade}^{-1}$ across the Maritime Continent region during March (not shown).

Models have significant omega trends across the tropical Indian Ocean that vary in sign and spatial extent, although increasing omega in the equatorial zone is the most common pattern. Where these patterns consist of zonal bands of descending and ascending trends, this may reflect changes to the location and/or strength of the convective band associated with the Inter-Tropical Convergence Zone (ITCZ); however, the zonal

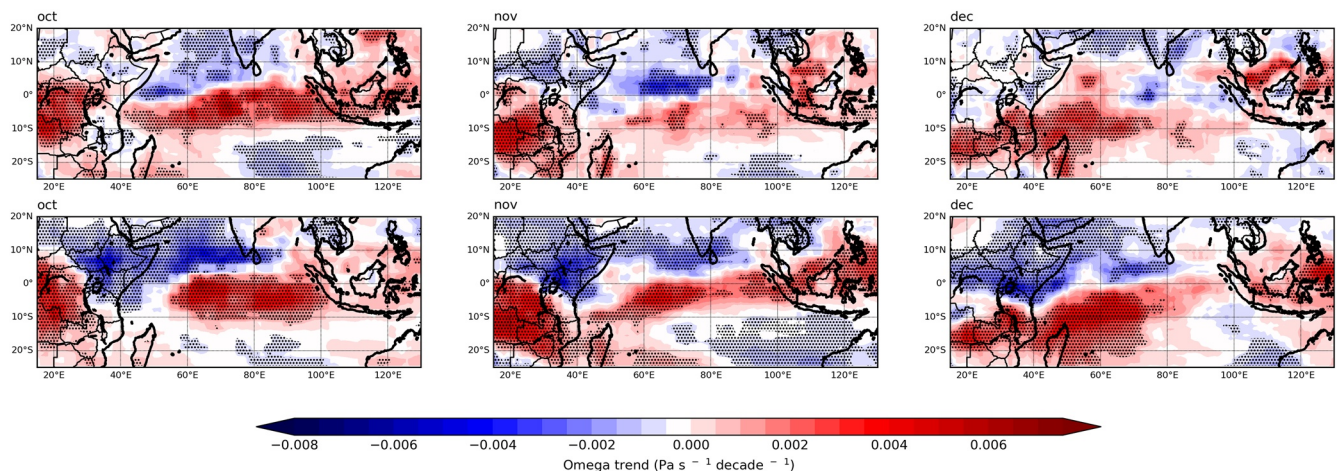


Figure 2. As Figure 1, but for October (left), November (middle), and December (right).

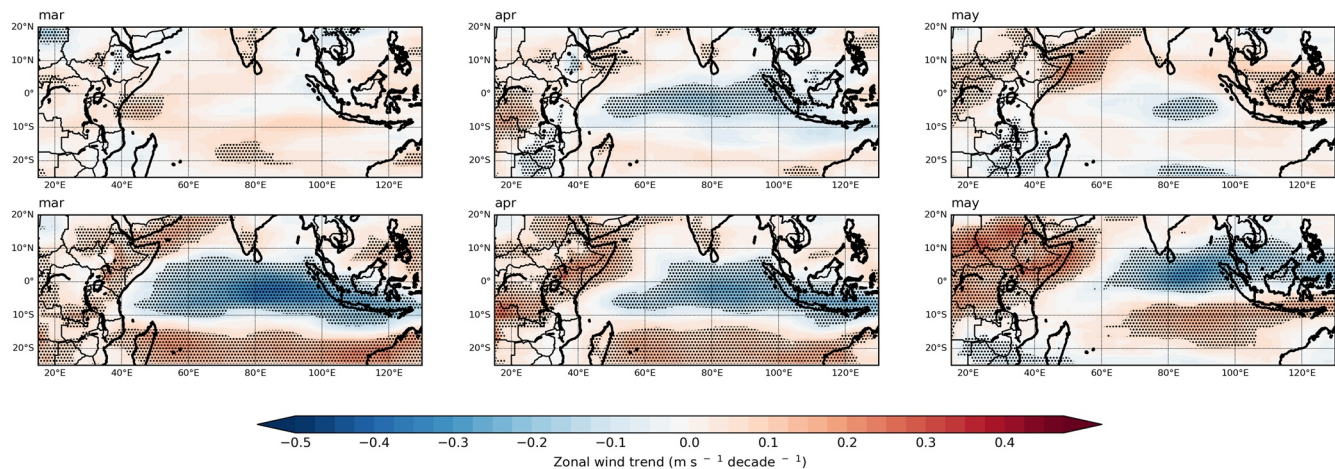


Figure 3. Linear regression trends in 850 hPa zonal wind for March (left), April (middle), and May (right), 2020–2100, under the RCP8.5 scenario. Stippling denotes areas where $p < 0.05$. For each month, the top 5 models with strongest drying/weakest wetting (top row) and strongest wetting (bottom row) are averaged to form a composite.

asymmetry of the general pattern across the Indian Ocean Basin in Figure 1 implicates the zonal IOWC as a driver of these vertical velocity trends.

Figure 2 shows the changes to 400 hPa omega projected under RCP8.5 during the short rains months. The general trend is for wetting models to have decreasing omega over Kenya which is absent from models with weak drying or no significant wetting. These omega decreases are more intense and more spatially extensive than in MAM ($\geq -0.006 \text{ Pa s}^{-1} \text{ decade}^{-1}$ over Kenya). In November and December, no models project significant drying over Kenya. This is reflected by weak but significant omega decreases over East Africa in the weakest wetting trend composites for these months ($\sim -0.002 \text{ Pa s}^{-1} \text{ decade}^{-1}$), and strong omega decreases in the strongest wetting models ($\geq -0.006 \text{ Pa s}^{-1} \text{ decade}^{-1}$). Ascent over East Africa is balanced by significant increasing omega trends ($\sim 0.004 \text{ Pa s}^{-1} \text{ decade}^{-1}$) over the Maritime Continent in both sets of composites. A consistent feature across the ensemble in October and November is extensive increasing omega trends with $p < 0.05$ over the eastern Congo Basin region.

Variation between models in the signs and locations of trend regions over the Indian Ocean itself suggest changes to circulation regimes in future continue to show a high contribution from model uncertainty.

3.1.3. Projected Changes in Zonal Winds

The role of the 850 hPa zonal winds over the equatorial Indian Ocean in advecting moisture toward the continent is important in determining East African rainfall variability (Nicholson, 2015). The representation of these winds is known to be a key source of CMIP5 rainfall biases during the East African short rains (Hirons & Turner, 2018), and any discussion of future projections of this variable must be interpreted in the context of the known biases during the short rains. The westerly winds form the return limb of the climatological IOWC.

Figures 3 and 4 show the linear trends in 850 hPa zonal wind up to 2100 under the RCP8.5 scenario. Significant zonal wind trends are present during the long rains, with increasing equatorial easterlies and continental westerlies predominating (Figure 3). These trends are stronger and more spatially extensive in the wetting composites, with easterly trends over the equatorial Indian Ocean reaching a magnitude of up to $-0.5 \text{ ms}^{-1} \text{ decade}^{-1}$. The easterly trends are absent from the drying/weak wetting composites in March, and are largely below the threshold for statistical significance in May. Similarly, there are significant westerly trends over continental East Africa in the wetting composites ($0.2\text{--}0.3 \text{ ms}^{-1} \text{ decade}^{-1}$) which are weaker and less significant in the drying/weak wetting composites. Given that these winds are moist, this could lead to enhanced moisture flux convergence with easterly winds from the Indian Ocean over East Africa. Changes to moisture flux convergence/divergence patterns at the East African margin of convection have been suggested by Giannini et al. (2018) as an explanation for future rainfall change in CMIP5.

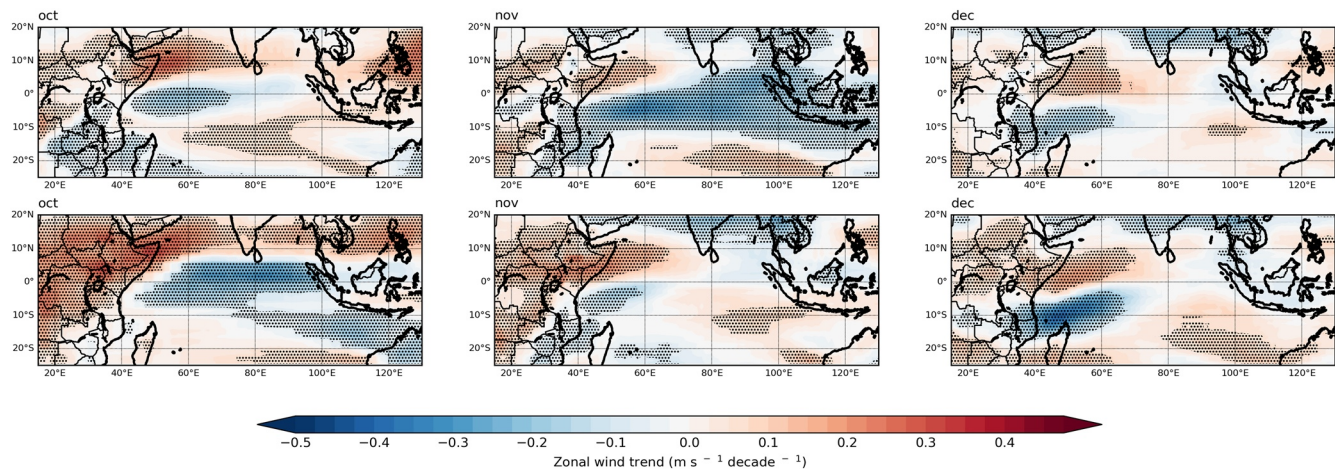


Figure 4. As Figure 3, but for October (Left), November (Center), and December (Right).

For the short rains months (Figure 4), the relationships between the zonal wind trends and rainfall trends are less clear in the model composites, and this is likely to reflect the idiosyncratic biases in model zonal wind direction during this season (Hirons & Turner, 2018). Models which are wet biased in historical runs already feature strong easterly winds over the equatorial Indian Ocean, and the trends in future wind speed may thus not be as significant an influence as the wind speed values themselves. For example, in October and November, the mean zonal wind bias over the equatorial Indian Ocean in the wettest 5 models is more easterly than in the driest 6 models: -3.50 ms^{-1} compared to -0.14 ms^{-1} for October and -2.20 ms^{-1} compared to -1.64 ms^{-1} in November. In October, models with strong wetting trends in future feature a characteristic pattern of significantly enhanced easterlies over the equatorial Indian Ocean and significantly enhanced westerlies over continental Africa, both of similar magnitude ($\pm 0.3 \text{ ms}^{-1} \text{ decade}^{-1}$). Both easterly and westerly trends are present in the drying/weak wetting composite but are reduced in magnitude and spatial extent, with no significant trends over Kenya and easterly trends only extending to around 70°E compared with 100°E in the strong wetting composite. In November, the weak wetting composite shows extensive easterly wind trends over the equatorial Indian Ocean, while these trends are confined to the East African coast in the wetting composite. This may reflect the presence of wetting across the ensemble in this month, as well as the wetting models already featuring strong easterly biases in historical runs when the climatological wind is westerly. Consequently, the wetting composite indicates where the increase in easterly winds is strongest, which is off the East African coast. For example, Hirons and Turner (2018) identify MRI-CGCM3 and ACCESS1-3 as models with strong easterly wind biases in the historical coupled models, with a bias relative to reanalysis of -2.79 ms^{-1} and -1.93 ms^{-1} respectively. These models also have strong historical wet biases over East Africa as a result. We find that both models continue to be wet in future, and as such are included in the composites for Figure 4. MRI-CGCM3 shows the strongest wetting trend of any model in the ensemble for November and the 4th wettest trend in December, and ACCESS1-3 has the 2nd strongest wetting trend in November and the 3rd strongest in December (Table 2). Conversely, models with (correct) westerly winds in historical runs would appear in the composite as having strong easterly trends if the westerlies are significantly reduced in strength in future. In December, the strong wetting and weak wetting composites show similar structures, with enhanced westerlies to the north of the equator over East Africa and easterlies to the south. While both composites show significant trends here, the trends are stronger by $0.1\text{--}0.2 \text{ ms}^{-1} \text{ decade}^{-1}$ in the strong wetting composite.

3.1.4. Projected Circulation Changes

King et al. (2020) link the rainfall biases over East Africa in historical runs of CMIP5 models to their representation of the overturning circulation over the equatorial Indian Ocean. Figures 5 and 6 show the composite differences in the same ensemble of models between a control period representing late 20th century conditions (1975–2005, historical coupled runs) and an end of 21st century period under the RCP8.5 scenario (2070–2100). For the long rains months (Figure 5), there are differences between the models show-

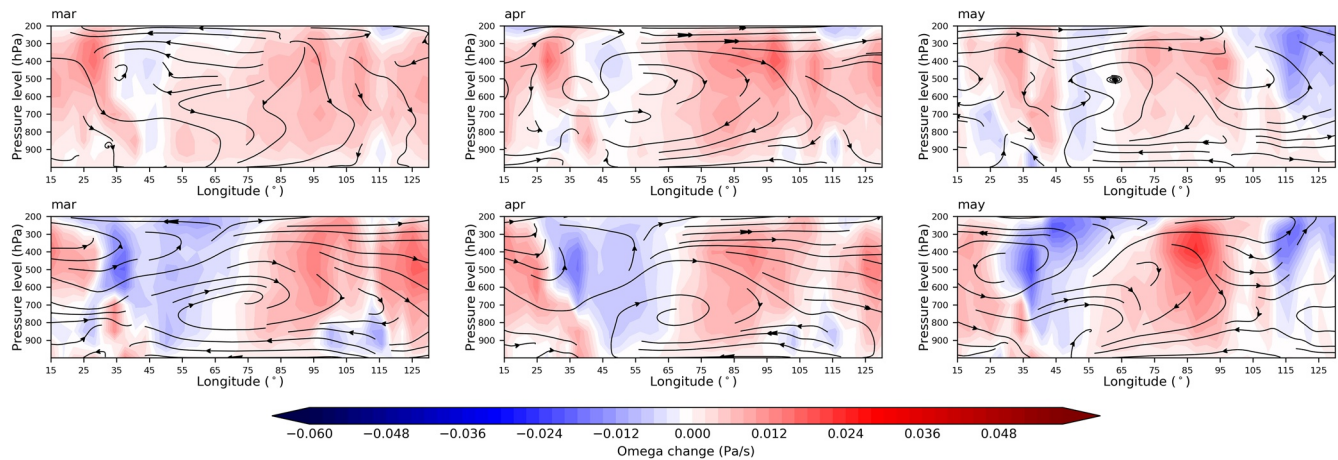


Figure 5. Longitude-height plots of the circulation over the equatorial Indian Ocean, 15°E–130°E, averaged over 5°N–5°S, for March (left), April (middle), and May (right). Shading is vertical velocity (ω) (Pa s^{-1}) with red indicating negative (upward) motion blue indicating positive (downward) motion. Streamlines are the resultant vectors of u and $\omega \times 10^4$. For each month, the means for 1975–2005 (historical coupled runs) are subtracted from the means for 2070–2100 (RCP8.5). For each month, the top 5 models with strongest drying/weakest wetting (top row) and strongest wetting (bottom row) are averaged to form a composite.

ing drying or weak wetting trends over Kenya (top rows) and those showing strong wetting trends (bottom rows). Principally, the changes to vertical velocity over East Africa and the western Indian Ocean are quantitatively different, with weak ascent throughout the troposphere in the weak wetting/drying composites of $> -0.01 \text{ Pa s}^{-1}$. In March, the 200 hPa wind trends are easterly, implying an enhancement of the upper-level branch of the Walker Circulation. By contrast, models with strong wetting trends show stronger and more spatially extensive negative omega composite differences over East Africa (-0.02 – -0.03 Pa s^{-1}). In these models, the changes in omega and streamlines reflect weakening of the zonal overturning, with reduced descent over East Africa and corresponding reduced ascent over the Maritime Continent, in both cases of magnitude $\sim \pm 0.03 \text{ Pa s}^{-1}$. The streamlines indicate enhanced lower-troposphere easterlies and upper-troposphere westerlies over the equatorial Indian Ocean, as well as enhanced westerly flow into East Africa from central Africa. The zonal pattern of omega changes (ascent over East Africa and descent over the Maritime Continent) is the reverse of the climatological direction of the IOWC.

In the short rains months (Figure 6), the changes to the overturning are also clearly distinct between the two sets of composites. For models with wetting trends in future, we see changes in overturning in opposition to the climatological IOWC, with streamlines indicating changes toward low-level equatorial easterly winds, and omega changes toward rising air over East Africa throughout the troposphere, and descent over the

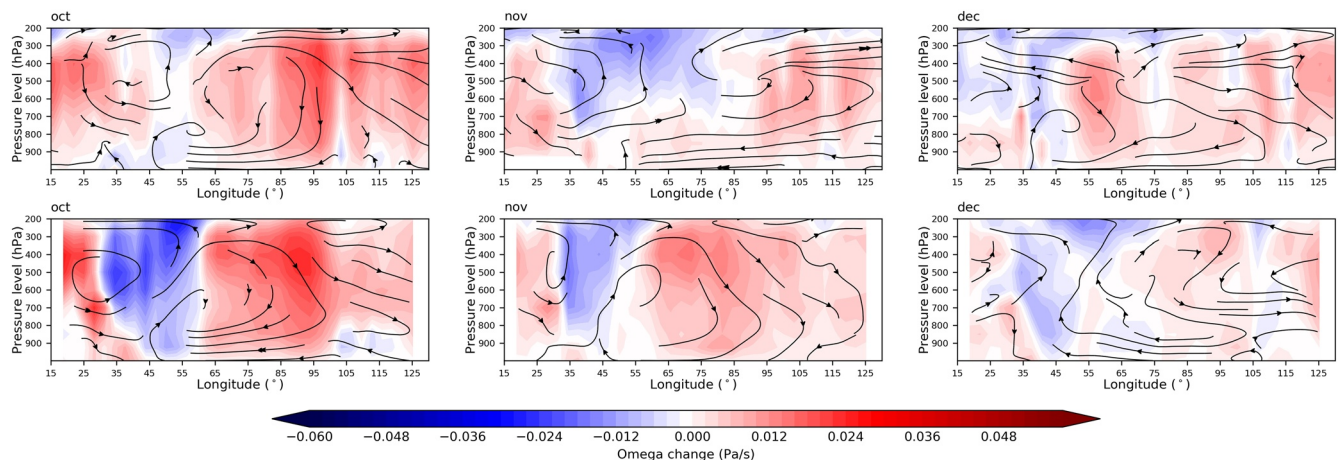


Figure 6. As Figure 5, but for October (left), November (middle), and December (right).

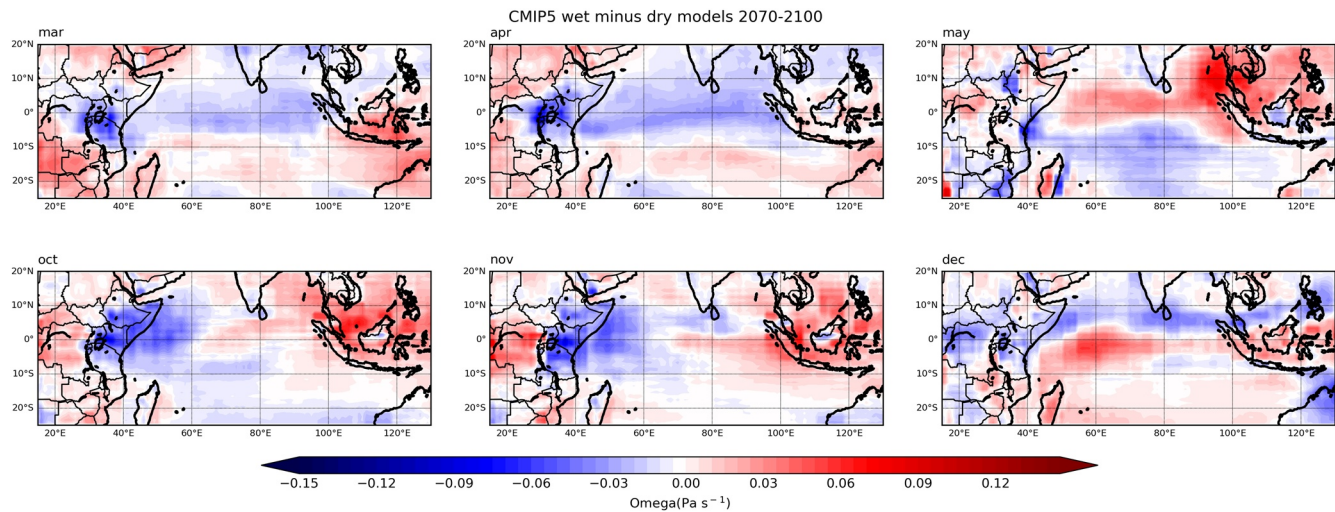


Figure 7. Wet minus dry model composites of 400 hPa omega, averaged over 2070–2100 under the RCP8.5 scenario.

Maritime continent. This demonstrates that the wetting trends in these models occur in conjunction with a weakening in the IOWC circulation consistent with wetter conditions over East Africa. The magnitude of the omega changes over both East African and the Maritime continent reach magnitudes of $\sim \pm 0.05 \text{ Pa s}^{-1}$, reflecting the stronger role of zonal overturning in the tropical climate during this season. The difference between the strong wetting and weak wetting composites are greatest in October, reflecting that wetting is more consistent across the ensemble in November and December (Table 2). Figures 5 and 6 show how the omega and zonal wind trends in Figures 1–4 are dynamically linked via the changes to the zonal overturning cell, and must be considered as part of the broader IOWC. Notably, the streamlines in the wetting composite for October, and in both sets of composites in November and December, show a trend toward low-level convergence over Kenya in wetting models, as westerly wind trends from the Congo Basin and easterly wind trends over the Indian Ocean meet at between 35°E and 45°E . This is associated with negative omega change from 900 hPa to 200 hPa. There is substantial variation between the models on the magnitude and zonal extent of positive omega change over the eastern part of the domain. While this change is present in most of the models, the magnitude varies from $<0.01 \text{ Pa s}^{-1}$ (INMCM4) to $>0.05 \text{ Pa s}^{-1}$ (CSIRO-Mk3-6-0) at the same location (95°E , 400 hPa) (not shown). This is reflected in the less strong descent in the composites relative to ascent over East Africa in Figure 7. This can be linked to the differing model behavior in the 1975–2005 baseline conditions; King et al. (2020) find that the equatorial overturning associated with the IOWC is not represented during this period in November in INMCM4, for example.

3.2. Links Between Historical Biases and Future Projections of IOWC Variables

The previous section has demonstrated that CMIP5 model projections, which are generally toward a wetter East Africa, occur concomitantly with changes to the IOWC including reduced positive omega and enhanced easterly winds. This supports other recent studies arguing that the IOWC is an important control on East African rainfall in both observations and models; it has been suggested that the dynamics control rainfall rather than the other way around (e.g., Chadwick et al., 2013; King et al., 2020; Mutai & Ward, 2000; Nicholson, 2017; Williams & Funk, 2011; Zhao & Cook, 2021), especially given the important role of SST in IOWC variability (Black, 2005; Hoell et al., 2017; Hoell & Funk, 2014; Liebmann et al., 2014). The important task that follows from this analysis is to assess the plausibility of these future projections in the context of the models' known biases in representation of the historical IOWC and associated rainfall conditions. This section addresses this by linking historical biases to future projections.

Table 3

Pearson Product Moment Correlation Coefficients Between CMIP5 Model Rainfall Averaged Over Kenya in Historical (1975–2005) and RCP8.5 (2070–2100) Runs of the CMIP5 Models Listed in Table 1

Month	March	April	May	October	November	December
R	0.854	0.851	0.882	0.908	0.821	0.673
R^2	0.730	0.724	0.778	0.825	0.674	0.453
p	0.0004	7.2E–08	5.5E–09	3.5E–10	4.9E–07	0.0002

3.2.1. Rainfall Change

We begin by assessing the extent to which CMIP5 models' historical precipitation over Kenya correlates with their future precipitation—in other words, are models that are particularly wet or dry in historical runs still particularly wet or dry in future projections under the RCP8.5 scenario? Table 3 shows the results of a correlation analysis comparing precipitation averaged over Kenya during 1975–2005 and 2070–2100, for each model in our ensemble ($n = 25$).

There are strong and significant correlations ($p < 0.001$) for each rainy season month between historical and projected rainfall over Kenya. For each month, models with rainfall >1 standard deviation above the ensemble mean for 1975–2005 also have rainfall >1 standard deviation above the ensemble mean in 2070–2100 (with the notable exception of GISS-E2-R, a wet model which projects drying trends in all rainy season months except March). Models which fulfill this condition for multiple months include ACCESS1-3 (October and November), BCC-CSM1-M (March and April), INMCM4 (March, April, October, and November), and MRI-CGCM3 (November and December). Conversely, models with rainfall >1 standard deviation below the ensemble mean in both time slices for multiple months include GFDL-CM3 (March and April) and, IPSL-CM5A-LR (October, November, and December). Since rainfall over East Africa in CMIP5 historical runs is known to be biased (Tierney et al., 2015) as the result of erroneous representation of regional dynamics (Hirons & Turner, 2018; King et al., 2020), the strong covariability between wet and dry models in both time slices implies similar processes may explain the spread in model rainfall projections. This is consistent with the comparatively time-invariant evolution of the model contribution to uncertainty in regional precipitation projections (Hawkins & Sutton, 2011).

3.2.2. Rainfall Versus Omega

Table 4A indicates that, apart from March, there are highly significant positive correlations during rainy season months between model vertical velocity over Kenya at 400 hPa in historical model runs and the RCP8.5 projections at the end of the 21st century for the same model ensemble. Correlations are more significant during the short rains months, when the IOWC is more active, especially during positive IOD events. This demonstrates that the sign and magnitude of model vertical velocity over Kenya in the historical period corresponds to that in the RCP8.5 projections. For example, models with omega values >1

Table 4

A. Pearson Product Moment Correlation Coefficients Between CMIP5 Model 400 hPa Omega Averaged Over Kenya in Historical (1975–2005) and RCP8.5 (2070–2100) Runs of the CMIP5 Models Listed in Table 1. B. Pearson Product Moment Correlation Coefficients Between Model Rainfall Change and 400 hPa Omega Change Over Kenya, 2070–2100 Minus 1975–2005

	Month	March	April	May	October	November	December
A.	R	0.041	0.871	0.798	0.930	0.909	0.865
	R^2	0.002	0.758	0.637	0.864	0.825	0.748
	p	0.844	1.5E–08	1.8E–08	1.9E–11	3.5E–10	2.4E–08
B. Omega change versus rainfall change							
	R	0.227	–0.878	–0.830	–0.795	–0.902	–0.679
	R^2	0.052	0.771	0.689	0.632	0.814	0.460
	p	0.275	8.0E–09	2.9E–07	2.0E–06	7.3E–10	0.0002

Table 5

A: Pearson Product Moment Correlation Coefficients Between CMIP5 Model 850 hPa Zonal Wind Averaged Over the Central Equatorial Indian Ocean in Historical (1975–2005) and RCP8.5 (2070–2100) Runs of the CMIP5 Models Listed in Table 1. B. Pearson Product Moment Correlation Coefficients Between Model Rainfall Change and 850 hPa Zonal Wind Change Over the Central Equatorial Indian Ocean, 2070–2100 Minus 1975–2005

A.	Month	March	April	May	October	November	December
	R	0.753	0.813	0.885	0.696	0.810	0.813
	R^2	0.568	0.662	0.784	0.484	0.650	0.660
	p	1.38E–05	7.7E–07	4.2E–09	0.0001	1.2E–06	0.8E–06
B.							
	R	–0.578	–0.482	–0.411	–0.586	–0.516	–0.419
	R^2	0.334	0.232	0.169	0.343	0.267	0.176
	p	0.002	0.01	0.04	0.002	0.008	0.04

standard deviation below the ensemble mean for both time slices include ACCESS1-3 (October and November), BCC-CSM1-1-M (all months except October), CNRM-CM5 (April, May, October, and November), GFDL-CM3 (November and December), and MRI-CGCM3 (October and November). Several of these models are also among the wettest for each month in both time slices, as shown above. Models with omega values > 1 standard deviation above the mean include BNU-ESM (April and May), CCSM4 (April and May), FIO-ESM (May, November, and December), IPSL-CM5A-LR (October, November, and December), and IPSL-CM5A-MR (October and November). These tend to be drier models. There is also a relationship across the model ensemble between the change in Kenya rainfall (as expressed by the composite difference between 2070–2100 and 1975–2005) and the change in 400 hPa vertical velocity between the same time slices (Table 4B). Apart from March, the correlations between these variables are statistically significant at $p < 0.05$ and strongly negative—models with increasing (decreasing) rainfall have decreasing (increasing) vertical velocity over Kenya. These results confirm the coherent behavior in CMIP5 models of the large scale circulation and rainfall over East Africa.

Figure 7 shows the differences in 400 hPa vertical velocity between the 4 wettest and 4 driest models for each rainy season month in the 2070–2100 time slice. Wet models in future are associated with negative omega (stronger ascent or weaker descent) over East Africa, with the strongest differences between wet and dry models seen over Kenya in March, April, October, and November. Conversely, wet models are also associated with positive omega (stronger descent or weaker ascent) over the Maritime continent, which is present in all rainy season months and strongest in May. The dipolar nature of the wet minus dry composites suggests a continued role for the IOWC in model projections of East African rainfall. The differing meridional gradients over the tropical Indian Ocean reflect the differing positions of the ITCZ over the Indian Ocean in each month. Wet models in March, April, and December feature increased ascent north of the equator, whereas in May there is increased ascent south of the equator. The zonal gradient between ascent and descent over the Indian Ocean is most pronounced in October and November, reflecting the increased activity of the IOD during these months (e.g., Deshpande et al., 2014).

3.2.3. Rainfall Versus Zonal Wind

Table 5A shows the strong and significant positive correlation between historical and future zonal winds over the central equatorial Indian Ocean (50°E–100°E, 5°N–5°S), a key contributing factor to historical model rainfall biases. We use the same area for averaging winds over the equatorial Indian Ocean as Hirons and Turner (2018) who first documented this bias in CMIP5 models. The results demonstrate that models featuring erroneously easterly winds during OND in the historical coupled runs continue to simulate easterlies in future. Models that do this include ACCESS1-3 (OND), BNU-ESM (D), CMCC-CM (OND), HadGEM2-AO (OND), and MRI-CGCM3 (OND). Although the zonal winds during the Long Rains have not been investigated in detail for CMIP5 in previous studies, our results show a similar pattern whereby easterly/westerly models continue to be so in future during March and April (all models feature westerly winds during May). Models disagree on the sign of the equatorial zonal winds during March and April during both time slices. Some models change sign from westerly to easterly winds between 1975–2005 and

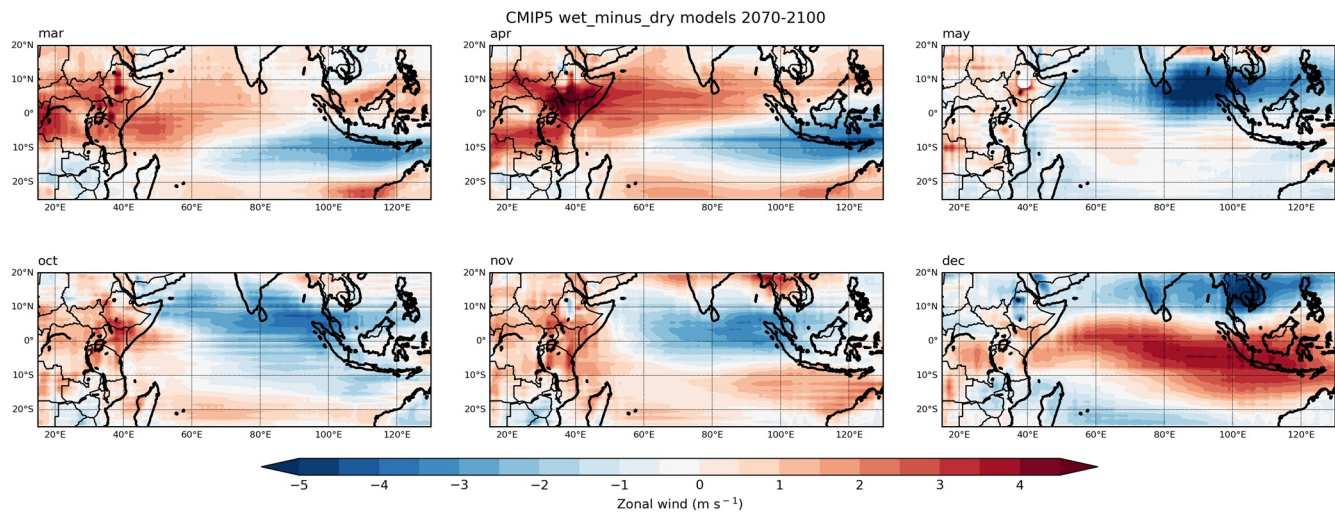


Figure 8. Wet minus dry model composites of 850 hPa zonal wind, averaged over 2070–2100 under the RCP8.5 scenario.

2070–2100: CNRM-CM5, GISS-E2-R, HadGEM2-AO, IPSL-CM5B-LR, and MRI-CGCM3 do this in March, and BNU-ESM and MIROC-ESM-CHEM do it in April. No models change from easterly winds to westerly winds. Table 5B also suggests a continued role for the 850 hPa zonal winds in driving projections of East African rainfall. Correlations between model rainfall change over Kenya and model zonal wind change over the equatorial Indian Ocean are significant at $p < 0.05$ and negative for all rainy season months. Because easterly wind values are negative in the zonal wind field, this implies that increasingly easterly zonal wind components in CMIP5 models are associated with increased rainfall over Kenya.

Figure 8 shows the differences in 850 hPa zonal wind between the dry and wet models for 2070–2100. During October and November, wet models have enhanced equatorial easterly wind over the Indian Ocean, consistent with the relationship between these winds and East African rainfall in historical models. In March and April, there are enhanced easterlies over the Indian Ocean at 10°S extending from the Maritime Continent into the central Indian Ocean, and enhanced westerlies on the equator extending to around 10°S. In May and December, wet models are associated with enhanced easterlies at 10°N, with strong westerlies on the equator in December. In all months, the wet minus dry composites show increasingly westerly winds over the East African landmass, particularly in March and April. Combined with patterns of enhanced easterlies over the Indian Ocean, this implies enhanced convergence of moist air masses (easterlies from the Indian Ocean and westerlies from the Congo Basin) at 850 hPa over East Africa in model projections, supporting the conclusions of Giannini et al. (2018) on the increasing importance of moisture flux from the Congo Basin in future East African rainfall. We also note that wet models show negative (easterly) signs over the Turkana Channel in northwestern Kenya, where the zonal wind field is dominated by the southeasterly Turkana LLJ. While most CMIP5 models are of insufficient resolution to represent this feature, higher-resolution ensemble members are able to simulate it (King et al., 2021). The westerly signs may reflect a slowing of low-level easterlies in wet model projections, which is consistent with some reanalysis datasets (King et al., 2021; Torralba et al., 2017).

3.2.4. Wet/Dry Future Composite Streamplots

Section 3.1 demonstrates that, for all rainy season months, the ensemble mean change is for increasing rainfall over Kenya, decreasing omega over Kenya, and enhanced easterly winds over the tropical Indian Ocean. Figure 9 reveals the structure of the overturning circulation in wet minus dry model composites, linking these findings together.

The differences between wet and dry models are evident in the residual overturning circulations. For all rainy season months, the wet composites feature negative omega over East Africa extending throughout the troposphere, indicating weakened descent/stronger ascent in this limb of the IOWC. Positive omega at lower levels (e.g., below 700 hPa over the East African continent between 35°E–45°E) may reflect divergence

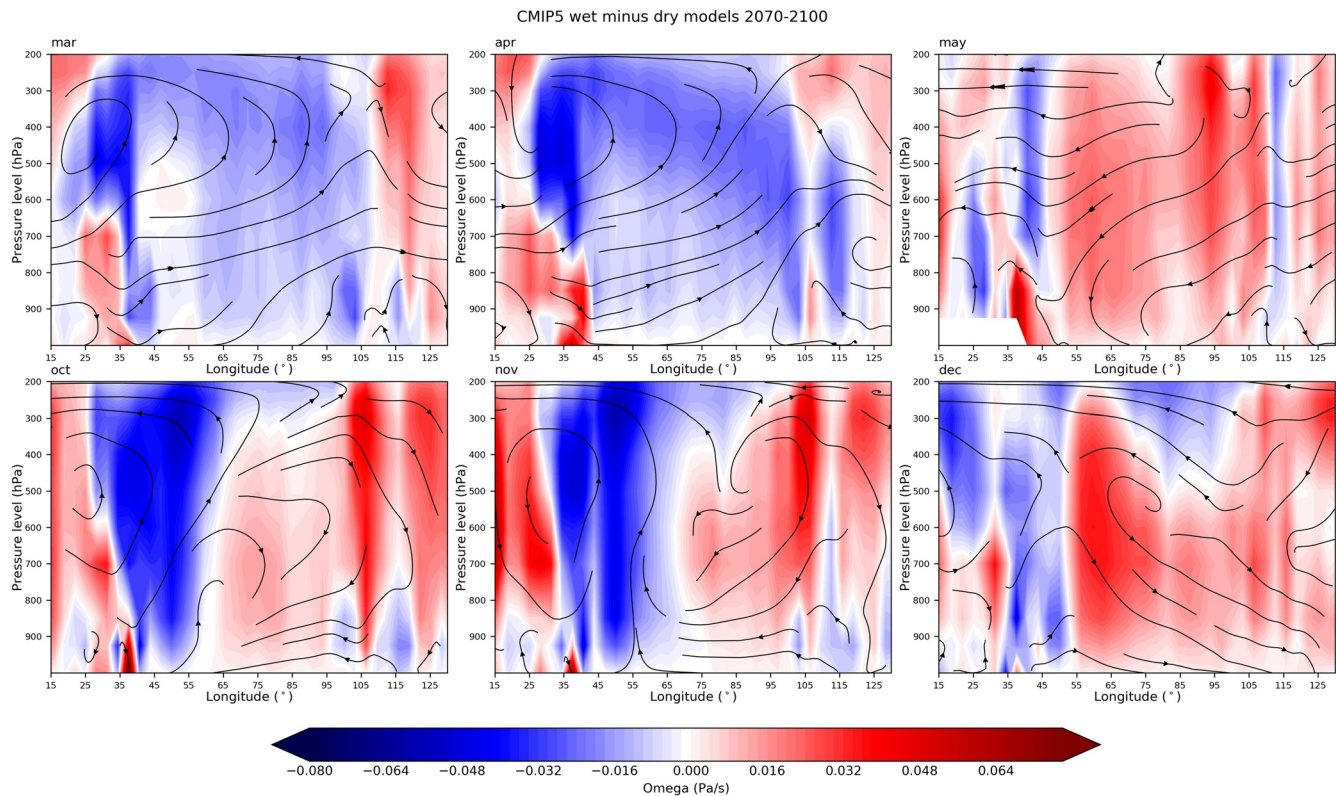


Figure 9. Wet minus dry model composites of the circulation over the equatorial Indian Ocean, averaged over 2070–2100 under the RCP8.5 scenario. Shading is vertical velocity (ω) (Pa s^{-1}) with red indicating negative (upward) motion and blue indicating positive (downward) motion. Streamlines are the resultant vectors of u and $\omega \times 10^4$.

from enhanced low-level westerly winds (Figures 3 and 4), while the extensive positive omega signs over the Indian Ocean in May, October, November, and December reflect the enhanced equatorial easterlies (Figures 5 and 6). Over the Maritime Continent, in the east of the domain, positive omega indicates a weakening of the ascending limb of the IOWC at this location (Figure 9), which extends throughout the troposphere and therefore suggests a reduction of deep convection over this region. Omega differences in both ascending and descending regions are strongest in October and November, and weakest in May and December. The streamlines link the zonal wind and omega changes to demonstrate a weaker IOWC in wet CMIP5 model projections. The changes in streamlines in October and November show this clearly, with the wet minus dry residual showing overturning acting in the opposite direction to the climatological IOWC.

3.3. Composite Projections

We next demonstrate an approach using metrics related to the dynamical structure of the IOWC to constrain CMIP5 projections of rainfall over Kenya and across East Africa. For each rainy season month in each model, we calculate the root mean square error (RMSE) of rainfall averaged over Kenya during 1981–2005 compared to the CHIRPSv2.0 data set (Funk et al., 2015). The time period chosen is a compromise between data availability for CHIRPSv2.0 and for CMIP5 historical coupled runs. We also calculate RMSE for omega averaged over Kenya at 400 hPa and zonal winds averaged over the central equatorial Indian Ocean at 850 hPa. For each RMSE calculation, we rank the models in order with from lowest to highest RMSE, and calculate the average rank across the three metrics. The 4 lowest and 4 highest scoring models for each month are selected to form ‘composite projections representing the top and bottom 16% of the ensemble. If a model that performs well otherwise has a mean 850 hPa central IO zonal wind value of the opposite sign to reanalysis, it is excluded from the composite and the next lowest scoring model with the correct zonal wind direction is included; however, this was only necessary for March. Table 6 shows the models used.

Table 6
CMIP5 Models Used to Produce Composites of Future Rainfall Following the Procedure Outlined in Section 3.3

Month	March	April	May	October	November	December
IOWC base state close to reanalysis	EC-EARTH	CMCC-CM	ACCESS1-3	CSIRO-Mk3-6-0	IPSL-CM5A-MR	EC-EARTH
	FIO-ESM	GISS-E2-R	CCSM4	FIO-ESM	MIROC5	IPSL-CM5A-LR
	INMCM4	INMCM4	IPSL-CM5A-LR	IPSL-CM5A-LR	MIROC-ESM-CHEM	IPSL-CM5A-MR
	NorESM1-M	MIROC-ESM-CHEM	MIROC-ESM-CHEM	MPI-ESM-MR	MPI-ESM-LR	MIROC-ESM-CHEM
IOWC base state deficient compared to reanalysis	BNU-ESM	BNU-ESM	BCC-CSM1-1-M	INMCM4	ACCESS1-3	BCC-CSM1-1-M
	CanESM2	IPSL-CM5B-LR	BNU-ESM	CNRM-CM5	CMCC-CM	CESM1-CAM5
	CSIRO-Mk3-6-0	MIROC5	FGOALS-g2	FGOALS-g2	GFDL-CM3	GISS-E2-R
	IPSL-CM5B-LR	MPI-ESM-MR	IPSL-CM5B-LR	MRI-CGCM3	MRI-CGCM3	INMCM4

3.3.1. Composite Trends

Figure 10 shows the differences between the rainfall projections for the composites during the long rains months. The changes are different in each month. For March, the low RMSE composite shows little change in rainfall between 2020 and 2100, with the linear regression model indicating an insignificant decrease (linear trend = $-0.016 \text{ mm day}^{-1} \text{ decade}^{-1}$, $p = 0.38$). By contrast, the high RMSE composite shows a significant increasing trend ($0.12 \text{ mm day}^{-1} \text{ decade}^{-1}$, $p = 1.2 \text{ E}^{-05}$), which results in the initially dry high RMSE models approximating the rainfall totals of the low RMSE models by 2100. For April, the low RMSE composite is wetter than the high RMSE composite and continues to be so throughout the 21st century by around 1 mm day^{-1} . Both composites show similar wetting trends that are just over the $p < 0.1$ criterion for statistical significance (low RMSE linear trend = $0.044 \text{ mm day}^{-1} \text{ decade}^{-1}$, $p = 0.11$, high RMSE linear trend = $0.033 \text{ mm day}^{-1} \text{ decade}^{-1}$, $p = 0.11$). In May, the low RMSE composite is consistently around 1.2 mm day^{-1} drier than the high RMSE composite. Both composites have small but significant wetting trends with $p < 0.1$, with that of the low RMSE composite being stronger (low RMSE linear trend = $0.081 \text{ mm day}^{-1} \text{ decade}^{-1}$, $p = 0.001$, high RMSE linear trend = $0.053 \text{ mm day}^{-1} \text{ decade}^{-1}$, $p = 0.094$).

There are also key differences between the low and high RMSE composites during the short rains months (Figure 11). For October, the high RMSE composite is consistently around 5 times wetter than the low RMSE composite. It also shows more interannual variability than the low RMSE composite (low RMSE standard deviation = 0.42 mm day^{-1} , high RMSE standard deviation = 0.99 mm day^{-1}). The low RMSE composite has a small but significant wetting trend at $p < 0.1$ ($0.038 \text{ mm day}^{-1} \text{ decade}^{-1}$, $p = 0.06$), whereas there is no trend in the high RMSE composite. For November, the high RMSE composite is again consistently wetter than the low RMSE composite by around 2 mm day^{-1} , with both composites showing wetting trends which are stronger in the high RMSE composite (low RMSE linear trend = $0.14 \text{ mm day}^{-1} \text{ decade}^{-1}$, $p = 9.7 \text{ E}^{-06}$, high RMSE linear trend = $0.24 \text{ mm day}^{-1} \text{ decade}^{-1}$, $p = 2.4 \text{ E}^{-05}$). In December, the picture is similar to November. The high RMSE composite is wetter than the low RMSE composite until 2100 by a consistent factor, and there are significant wetting trends in both composites (low RMSE linear trend = $0.09 \text{ mm day}^{-1} \text{ decade}^{-1}$, $p = 3.8 \text{ E}^{-05}$, high RMSE linear trend = $0.08 \text{ mm day}^{-1} \text{ decade}^{-1}$, $p = 0.006$).

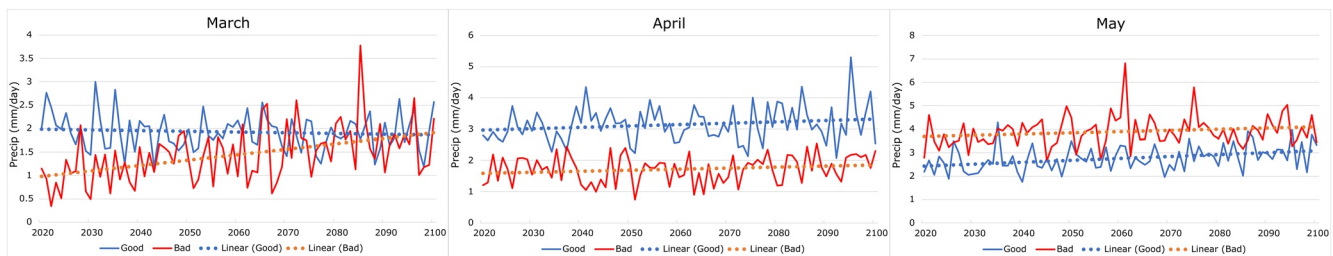


Figure 10. Rainfall projections over Kenya from the low root mean square error (RMSE) 'good' (blue) and high RMSE 'bad' (red) model composites shown in Table 6 for March–April–May (MAM), over 2020–2100 under RCP8.5. The dotted line is a linear regression model fitted to each composite time series. Note different y axis scales.

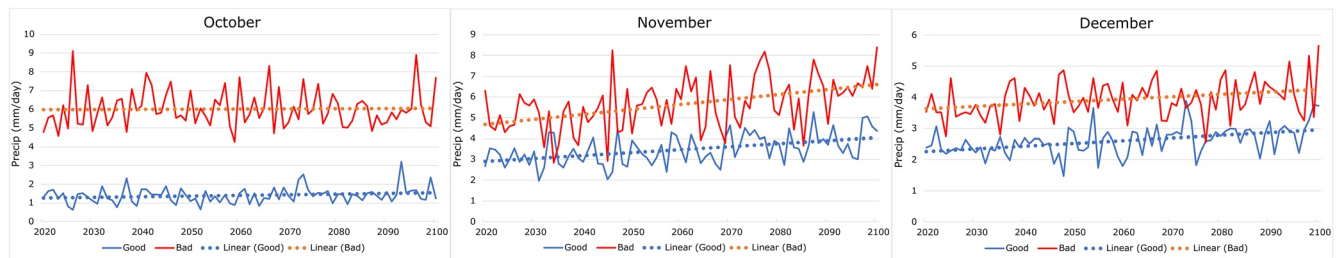


Figure 11. As Figure 10 but for OND. Note different y axis scales.

3.3.2. Composite Trend Maps

Figures 12 and 13 show the spatial patterns of the future rainfall trends in the low RMSE and high RMSE composites. Although our analysis focuses on Kenya, an accurate representation of the IOWC should result in more plausible future rainfall projections across East Africa.

In March, the only significant rainfall trends over Kenya in the low RMSE composite are found in the extreme east of the country, as part of an area of decreasing rainfall extending across southern Ethiopia and

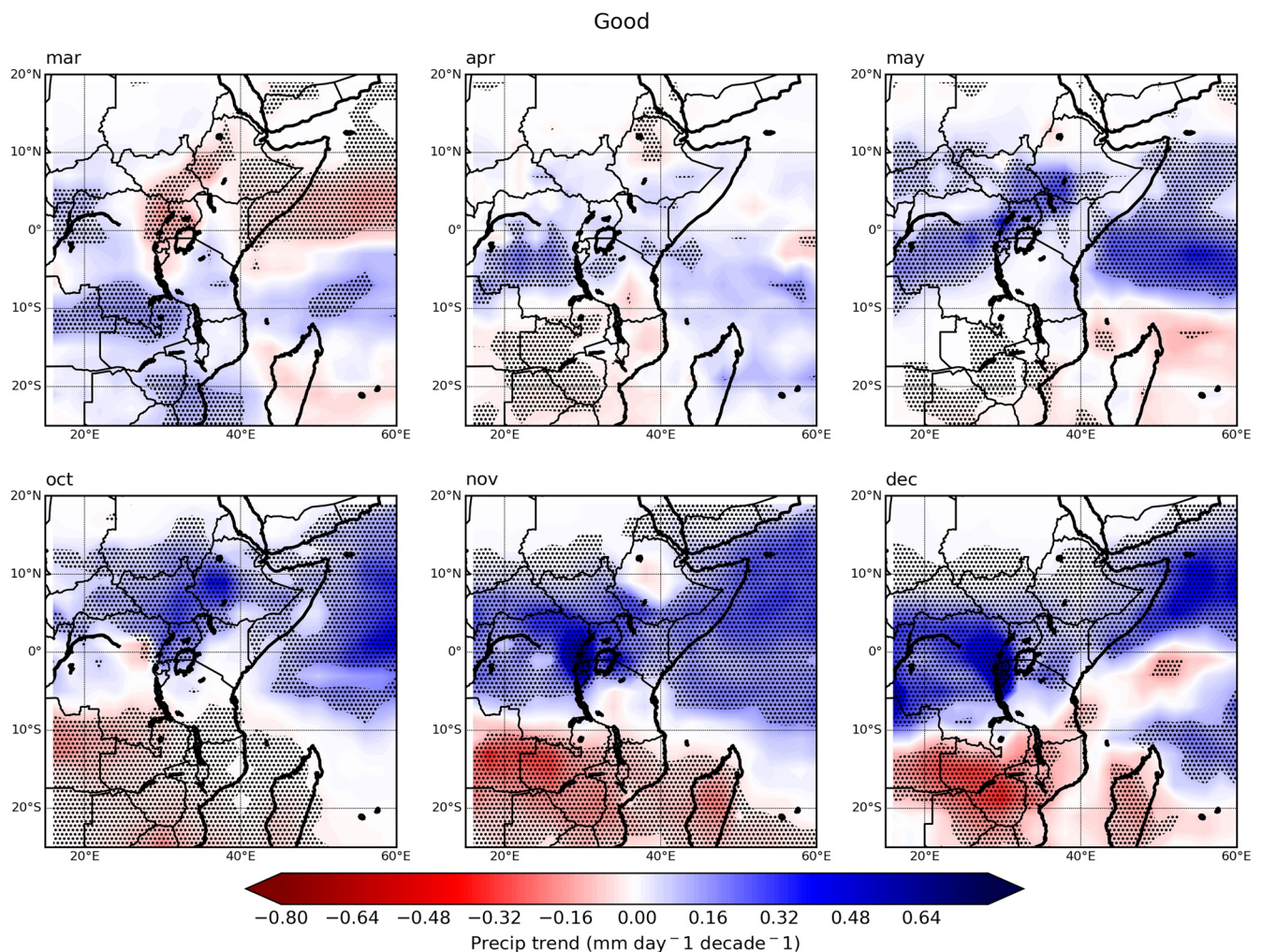


Figure 12. Linear regression trends of precipitation over East Africa for the low RMSE composites listed in Table 5, 2020–2100, RCP8.5. Stippling indicates significance at $p < 0.1$.

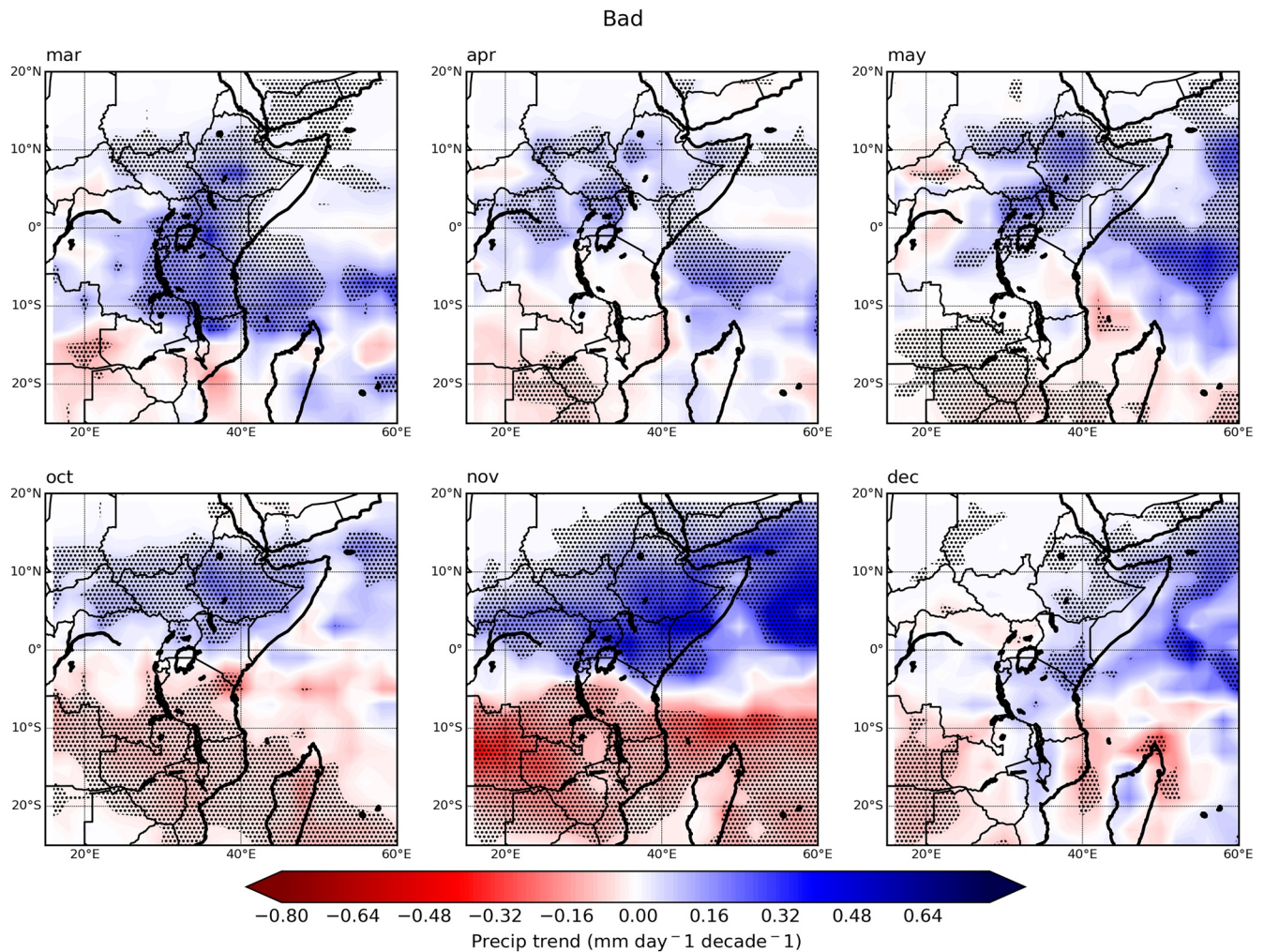


Figure 13. As Figure 12, but for the high root mean square error (RMSE) composites listed in Table 6.

Somalia. Significant drying is also seen in western Ethiopia, South Sudan, and Uganda. Wetting trends are found inland in the Congo Basin area (as in all rainy season months except October), and across northern Angola, and Zambia. In April, there are fewer significant trends in the Greater Horn of Africa, with weak wetting in Kenya and southern Ethiopia. May features stronger wetting trends in northern and central Kenya, southern Ethiopia, Uganda, and South Sudan, with a band of wetting extending from the Congo Basin and further wetting over the equatorial Indian Ocean (Figure 12).

The short rains are characterized by a strong meridional gradient between wetting north of 10°S and drying south of it. Stronger trends are found for the short rains months than the long rains. In October the strongest wetting trends are found over the Ethiopian Highlands, while in November and December they are found to the west of Lake Victoria along the DRC's borders with Uganda, Rwanda, and Tanzania. Only the northern tip of Kenya experiences a significant wetting trend in October, but wetting is evident across the whole country in November and December. The Ethiopian Highlands experience a weak drying trend in November, in contrast to the other short rains months.

Figure 13 shows the spatial patterns of RCP8.5 rainfall change in the high RMSE model composites. In March, there is an extensive and significant increase in rainfall across East Africa, in contrast to the drying signal seen in the low RMSE composite (Figure 12). The wetting covers all of Kenya, and most of Ethiopia, South Sudan, Uganda, Rwanda, and Tanzania. There is also no significant wetting over the Congo Basin, unlike in the low RMSE composite. In April, wetting is seen in South Sudan and northwestern Kenya, as

well as in western Ethiopia which gets drier in the low RMSE composite. There are rainfall increases over the Congo Basin but these are mostly to the north of the basin, as opposed to the center in the low RMSE composites. In May, the high RMSE composite features extensive wetting over central Ethiopia but not the Congo Basin, in contrast to the low RMSE composite, but the pattern of rainfall change over Kenya is similar with increases concentrated in the Turkana region.

For the short rains months, the high RMSE composite also features a meridional divide between wetting to the north and drying to the south, but the dividing latitude is further north ($\sim 5^{\circ}\text{S}$). In October, there is significant wetting in northern Kenya and drying in southern Kenya. The strongest wetting is located further east over Ethiopia than in the low RMSE composite, and there is much less wetting over the northwest Indian Ocean. In November, there is a stronger wetting trend across East Africa, including over areas of Ethiopia where the low RMSE composite shows drying. The wetting area over the Congo Basin is shifted to the north. In December, trends are less extensive than in the low RMSE composite, with increasing rainfall in southern Kenya, but no significant trends across South Sudan and the Congo Basin where strong wetting is seen in the low RMSE composite.

4. Discussion

We demonstrate that the general wetting trends projected for East Africa in the means of large CMIP5 ensembles do not capture the spread of model projections, in particular for the long rains months where trends are equivocal. The different trends seen in different months of the rainy seasons demonstrate the limitations of taking seasonal averages (Nicholson, 2017). For example, during the long rains, not all models project increasing East African rainfall—the condition leading to the ‘climate paradox’ (Rowell et al., 2015). Although the ensemble mean rainfall trend is statistically significant for all months, only one model in the ensemble (IPSL-CM5A-LR) has significant trends in all months; conversely, a single model, GISS-E2-R, has no significant rainfall trends during the rainy seasons in Kenya during the 21st century. Three models have a significant rainfall decline in May until 2100. The precipitation increases projected for the short rains were robust across the ensemble (at least during ON), but models disagreed on which month had the more significant rainfall increase. We note that models which are wet (dry) over Kenya in historical runs tend to be wet (dry) in RCP8.5 projections. The majority of models in our ensemble do not have significant rainfall trends during MAM. Therefore, the ensemble mean rainfall averages for both historical and future simulations of the long rains are thus dominated by a few very wet or very dry models. The wet biased models in MAM could be considered more realistic, as the ensemble mean has a dry bias during the season, but King et al. (2020) have shown that these highly biased models have unrealistic dynamics over East Africa and the tropical Indian Ocean in the historical coupled simulations.

In this case where a complex regional climate poses simulation challenges, it is necessary to constrain projections using a process-based methodology that takes into account the differing representation of key regional dynamics (Dyer et al., 2020; McSweeney et al., 2015; Rowell et al., 2016). We use an approach based on previous work linking model representation of the IOWC to historical rainfall biases. We first demonstrate that, as for rainfall, models with particularly strong (weak) IOWCs (as evidenced by vertical velocity over Kenya and zonal wind over the equatorial Indian Ocean) in historical runs continue to feature these biases in RCP8.5 projections. We show the links between changes to IOWC dynamic fields (both vertical velocity and zonal wind) and changes to rainfall over Kenya. We also demonstrate that changes in these IOWC variables are strongly linked to the magnitude of model rainfall change in future. This is in line with work by others arguing that the magnitude (Chadwick et al., 2013) and spatial patterns (Pfahl et al., 2017) of future tropical rainfall change are determined by changes to regional dynamics. It remains a challenge to constrain model ensembles in regions such as East Africa, where model performance is generally low and where the ensemble mean may not be plausible (Dyer & Washington, 2021). This study does not provide a comprehensive answer to the outstanding questions of whether a wetter or a drier future is likely; by definition, different sets of model evaluation metrics will yield different results (e.g., Dyer & Washington, 2021; McSweeney et al., 2015; Ongoma et al., 2019; Rowell et al., 2016). Rather, it aims to contribute to a growing literature that provides a model evaluation ‘toolkit’, in which multiple approaches can be synthesized to enable model projections to be selected based on specific research questions rather than convenience (James et al., 2018).

It is acknowledged that the use of omega to diagnose rainfall in models is complicated in the tropics by the approximate equivalence between omega and diabatic heating. However, the picture over Kenya is unusual relative to much of the tropical land because of the lack of deep convective rainfall, at least in part as a result of its location underlying a descending limb of the IOWC (Nicholson, 2017). In this sense, omega and associated divergence over Kenya is reflective of a process which inhibits precipitation rather than precipitation itself, which has enabled the use of omega as a diagnostic for both reanalysis and modeling studies of tropical African rainfall (e.g., Creese, Washington, & Jones 2019; Creese, Washington, & Munday, 2019; Dyer & Washington, 2021; Hastenrath et al., 2007; Hoell & Funk, 2014; Mutai et al., 2012).

The relationship between wetting and low-level continental westerlies implies that changes to the overturning circulation over the Congo Basin are important in future. The relative strength of each overturning cell, and the location of the region of maximum zonal convergence over East Africa, could therefore be an important determinant of future East African rainfall (Creese, Washington, & Jones 2019; Creese, Washington, & Munday, 2019; Giannini et al., 2018; Zhao & Cook, 2021).

Increasing omega trends over the eastern Congo Basin are consistent with the changes to local overturning in the Congo Basin found by Creese, Washington, and Jones (2019) and Creese, Washington, and Munday (2019) across wet and dry models in that domain, although a lack of representation of the African Easterly Jet (AEJ) in CMIP5 historical coupled runs casts some doubt on model projections in this region (Creese, Washington, & Jones 2019; Creese, Washington, & Munday, 2019). The general pattern of omega decrease to the north of the domain and increase to the south is suggestive of a northward shift of the zone of maximum tropical convergence (Creese, Washington, & Jones 2019; Creese, Washington, & Munday, 2019).

Fereday et al. (2020) have recently argued that tropical rainfall will also have an increasing dynamic impact on extratropical climate, meaning that an understanding of tropical rainfall dynamics is essential for both near-term predictability and longer-term climate projections on increasingly large spatial scales. We therefore consider these process-based assessments of rainfall projections to be essential for other parts of the tropics, and they must be used for the new CMIP6 model generation. Early results have suggested limited improvements between CMIP5 and CMIP6 in representation of East African rainfall (Ayugi et al., 2021) and the IOD (McKenna et al., 2020) and the atmospheric consequences of the latter in particular requires further investigation. The question of whether the IOD controls the IOWC or vice versa remains unresolved (Baba, 2020; Yang et al., 2020).

The projections and composites indicate an important role for 850 hPa zonal winds and 400 hPa omega in future East African rainfall, which constitute metrics of the IOWC system. These variables are an important source of uncertainty in future projections because of their erroneous representation in historical models (Hirons & Turner, 2018; King et al., 2020). We show that wet minus dry composites in future feature enhanced ascent over East Africa and reduced ascent over the Maritime Continent. Wet models tend toward equatorial easterlies in ON, with stronger easterlies in the southern tropical IO in March–April and in the northern tropical IO in May and December. However, these wet composites, especially for OND, may not be plausible owing to the continuity between wet-biased models featuring erroneous zonal winds in historical runs and these same models being wet in future. For example, of the 4 wettest models in 2070–2100 for ON, 3 had mean-state easterly zonal winds in 1975–2005 where reanalysis datasets indicate westerlies. Models tend to have stronger easterlies in the region of the Turkana low-level jet (Kinuthia & Asnani, 1982) in MAM rather than OND. This may contribute to the models' rainfall biases in the respective seasons, given the links between the jet and regional aridity in northern Kenya (Nicholson, 2016), and the tendency for many models to simulate easterlies at the equator in OND, which could reduce the momentum flux into the Turkana Channel (Hartman, 2018). Our results also indicate that strengthening westerly winds over East Africa at 850 hPa are associated with wetter conditions over East Africa in RCP8.5, with a westerly wet minus dry composite for 2070–2100 over the region. This supports findings from Dyer and Washington (2021) on the increasing importance of moisture flux from the Congo Basin into East Africa, and the link between low-level westerlies and East African rainfall found by Walker et al. (2020); however, CMIP5 model dynamics over the Congo Basin have been called into question in a number of studies (Creese & Washington, 2016, Crowhurst et al., 2020; Washington et al., 2013). Combined with enhanced tropical easterlies over the Indian Ocean, these enhanced westerlies would increase moisture flux convergence over Kenya. This may also reflect a decrease in the strength of the Turkana low-level jet in future (King et al., 2021). Future work on

East African climate should investigate the representation of the Walker Circulation cell over the Congo Basin, including the impact of parameterized processes (Crowhurst et al., 2020; Jackson et al., 2020).

Our results also highlight the importance of model topography and resolution in simulating Walker Circulation controls on East African rainfall. Kenya in particular underlies an area of climatological descending air in the mid-troposphere, with ascending air to the west (Congo Basin) and east (Indian Ocean). The location of the margins between these zones can determine the rainfall received over East Africa in climate models. The omega trend plots show how East Africa is also a zone of transition between areas of increasing negative omega (Congo Basin) and increasing positive omega (Indian Ocean). Representation of the topography of the East African highlands is therefore important, as the mountain ranges act as a barrier between these large-scale change regions; the Walker Circulation has been shown to be sensitive to model topography in CMIP5 models (Naiman et al., 2017). Reinforcing the argument that tropical precipitation changes will be determined by shifts in the location of convergence zones (Chadwick et al., 2013), we argue that greater attention needs to be paid to topography in GCMs, particularly in areas of the tropics with complex relief. This is an area where high-resolution regional modeling can add value, particularly where explicit convection is available (e.g., Stratton et al., 2018), and this approach is already yielding improvements (Finney et al., 2019); but care needs to be taken in the selection of the driving GCM given that zonal wind and moisture flux errors propagate into the RCM as boundary conditions.

Finally, our results have important impacts for future East African rainfall and the issue of the “climate paradox.” Fewer than half of the models in our ensemble projected significant rainfall increase in the long rains months. By constraining projections using metrics of the IOWC, we find that models with a good simulation of the structure of the overturning circulation over the Indian Ocean show no significant increases in rainfall over Kenya in 2/3 long rains months, and indeed widespread decreases in rainfall across East Africa in March. By contrast, models with inaccurate dynamics show strong wetting trends in March, in opposition to the low RMSE models, and more spatially extensive wetting in April and May. This suggests that the ‘climate paradox’ may be at least partially attributable to increasing rainfall in models with unrealistic representations of the IOWC. The low RMSE composite rainfall increases are concentrated in April/May, implying a shift toward a later rainy season which aligns with projections of increased summer rainfall in CMIP5 (Yang et al., 2015) and a later onset of observed MAM rainfall (Wainwright et al., 2019). This also demonstrates that an approach based on seasonal rainfall averages is not sufficient. The increase in short rains rainfall appears robust in November and December, but high RMSE models are much wetter throughout the 21st century and also have stronger wetting trends. We therefore call into question the ensemble mean rainfall projections in the CMIP5 models, but provide a process basis for assessing the plausibility of projections from individual models that implies a reduced rainfall increase in April and May and a stronger wetting signal in November and December for the remainder of the 21st century under a high warming scenario.

5. Conclusions

This article addresses three main questions. First, we determined the rainfall changes projected over Kenya up to 2100 by CMIP5 models under the RCP8.5 scenario for each month in the two rainy seasons. We showed that there is substantial variation between models, and that the most robust trend is toward increasing rainfall in October and November. We also showed how these rainfall changes are dynamically linked to the IOWC, with model rainfall increases associated with a weaker overturning circulation as evidenced by changes to vertical velocity over East Africa (decreasing) and the Maritime Continent (increasing), and enhanced westerly flow over the equatorial Indian Ocean. Second, we demonstrated relationships between historical model biases and future trends in rainfall and IOWC fields, and between the magnitude of future changes in rainfall and IOWC fields, across the rainy season months. This demonstrated that processes linked to model biases in the past are associated with model performance in the future. Third, we used simple metrics of model IOWC representation to constrain rainfall projections, demonstrating that the future of East African rainfall is quantitatively different depending on whether the models selected have realistic or unrealistic IOWC representation. Our results have important implications for East African climate, suggesting that the long rains rainfall increase projected by the ensemble mean, and the resulting ‘climate paradox’, may result from the disproportionate influence of models with strong wet signals resulting from unrealistic

IOWC representation. Smaller rainfall increases later in the season may be a more likely outcome by 2100. Conversely, we find that increasing short rains rainfall is a feature of models with accurate IOWCs, but the spatial patterns vary. The influence of the Congo Basin as a source of moisture needs further investigation, as does the role of model topography in determining the location of future margins of ascent and descent. These results will be useful to help choose GCMs for use in downscaling experiments and impact modeling, and therefore contribute to the evidence basis for climate change impact planning in East Africa. Looking forward to CMIP6, we argue that similar process-based evaluations be carried out to determine the role of IOWC biases in future projections, including elsewhere in the tropics, and particularly the Congo Basin. Finally, agreement on a definition of the IOWC would improve the efficiency of these assessments.

Data Availability Statement

The CMIP5 data used in this study were downloaded from the UK Centre for Environmental Data Analysis (CEDA), (<https://catalogue.ceda.ac.uk/uuid/d2d8f982d66cce55bb59fc769ca39264?jump=related-docs-anchor>). MERRA-2 data were downloaded from the NASA Goddard Earth Sciences Data and Information Services Centre (<https://disc.gsfc.nasa.gov/datasets?keywords=%0022MERRA-2%22&page=1&source=Models%2FAnalyses%20MERRA-2>). CHIRPS data were downloaded from the Climate Hazards Group at the University of California, Santa Barbara (<https://data.chc.ucsb.edu/products/CHIRPS-2.0/>).

Acknowledgments

James A. King is funded by the UK Natural Environment Research Council (NERC) through the Doctoral Training Partnership in Environmental Research (grant NE/L002621/1). This work forms part of his doctoral thesis. The authors thank Ellen Dyer and Neil Hart for useful discussions.

References

- Ayugi, B., Jiang, Z., Zhu, H., Ngoma, H., Babausmail, H., Karim, R., & Dike, V. (2021). Comparison of CMIP6 and CMIP5 models in simulating mean and extreme precipitation over East Africa. *International Journal of Climatology*. <https://doi.org/10.1002/joc.7207>
- Baba, Y. (2020). Roles of atmospheric variabilities in the formation of the Indian Ocean Dipole. *Ocean Dynamics*, 70, 21–39. <https://doi.org/10.1007/s10236-019-01318-7>
- Behera, S. K., Luo, J.-J., Masson, S., Delecluse, P., Gualdi, S., Navarra, A., & Yamagata, T. (2005). Paramount impact of the Indian Ocean Dipole on the East African short rains: A CGCM study. *Journal of Climate*, 18, 4514–4530. <https://doi.org/10.1175/JCLI3541.1>
- Berhane, F., & Zaitchik, B. (2014). Modulation of daily precipitation over East Africa by the Madden-Julian Oscillation. *Journal of Climate*, 27, 6016–6034. <https://doi.org/10.1175/JCLI-D-13-00693.1>
- Black, E. (2005). The relationship between Indian Ocean sea-surface temperature and East African rainfall. *Philosophical Transactions of the Royal Society A*, 363, 43–47. <https://doi.org/10.1098/rsta.2004.1474>
- Borgomeo, E., Vadheim, B., Woldeyes, F. B., Alamirew, T., Tamru, S., Charles, K. J., et al. (2018). The distributional and multi-sectoral impacts of rainfall shocks: Evidence from computable general equilibrium modelling for the Awash Basin, Ethiopia. *Ecological Economy*, 146, 621–632. <https://doi.org/10.1016/j.ecolecon.2017.11.038>
- Cai, W., & Cowan, T. (2013). Why is the amplitude of the Indian Ocean Dipole overly large in CMIP3 and CMIP5 models? *Geophysical Research Letters*, 40, 1200–1205. <https://doi.org/10.1002/gri.50208>
- Chadwick, R., Boutle, I., & Martin, G. (2013). Spatial patterns of precipitation change in CMIP5: Why the rich do not get richer in the tropics. *Journal of Climate*, 26, 3803–3822. <https://doi.org/10.1175/JCLI-D-12-00543.1>
- Cook, K. H., Fitzpatrick, R. G. J., Liu, W., & Vizi, E. K. (2020). Seasonal asymmetry of equatorial East African rainfall projections: Understanding differences between the response of the long rains and the short rains to increased greenhouse gases. *Climate Dynamics*. <https://doi.org/10.1007/s00382-020-05350-y>
- Creese, A., & Washington, R. (2016). Using gflux to constrain modeled Congo Basin rainfall in the CMIP5 ensemble. *Journal of Geophysical Research - D: Atmospheres*, 121(13), 442. <https://doi.org/10.1002/2016JD025596>
- Creese, A., Washington, R., & Jones, R. (2019). Climate change in the Congo Basin: Processes related to wetting in the December–February dry season. *Climate Dynamics*, 53, 3583–3602. <https://doi.org/10.1007/s00382-019-04728-x>
- Creese, A., Washington, R., & Munday, C. (2019). The plausibility of September–November Congo Basin rainfall change in coupled climate models. *Journal of Geophysical Research Atmospheres*, 124, 5822–5846. <https://doi.org/10.1029/2018JD029847>
- Crowhurst, D. M., Dadson, S. J., & Washington, R. (2020). Evaluation of evaporation climatology for the Congo Basin wet seasons in 11 global climate models. *Journal of Geophysical Research - D: Atmospheres*, 125, e2019JD030619. <https://doi.org/10.1029/2019JD030619>
- Deshpande, A., Chowdary, J. S., & Gnanaseelan, C. (2014). Role of thermocline–SST coupling in the evolution of IOD events and their regional impacts. *Climate Dynamics*, 43, 163–174. <https://doi.org/10.1007/s00382-013-1879-5>
- Diro, G. T., Grimes, D. I. F., & Black, E. (2010). Teleconnections between Ethiopian summer rainfall and sea surface temperature: Part I—Observation and modelling. *Climate Dynamics*, 37, 103–119. <https://doi.org/10.1007/s00382-010-0837-8>
- Dunning, C. M., Black, E. C. L., & Allan, R. P. (2016). The onset and cessation of seasonal rainfall over Africa. *Journal of Geophysical Research - D: Atmospheres*, 121, 11405–11424. <https://doi.org/10.1002/2016JD025428>
- Dyer, E., & Washington, R. (2021). Kenyan long rains: A subseasonal approach to process-based diagnostics. *Journal of Climate*, 34, 3311–3326. <https://doi.org/10.1175/JCLI-D-19-0914.1>
- Dyer, E., Washington, R., & Teferi Taye, M. (2020). Evaluating the CMIP5 ensemble in Ethiopia: Creating a reduced ensemble for rainfall and temperature in Northwest Ethiopia and the Awash basin. *International Journal of Climatology*, 40, 2964–2985. <https://doi.org/10.1002/joc.6377>
- Endris, H. S., Lennard, C., Hewitson, B., Dosio, A., Nikulin, G., & Artan, G. A. (2018). Future changes in rainfall associated with ENSO, IOD and changes in the mean state over Eastern Africa. *Climate Dynamics*, 52, 2029–2053. <https://doi.org/10.1007/s00382-018-4239-7>
- Fereday, D. R., Chadwick, R., Knight, J. R., & Scaife, A. A. (2020). Tropical rainfall linked to stronger future ENSO–NAO teleconnection in CMIP5 models. *Geophysical Research Letters*, 47, e2020GL088664. <https://doi.org/10.1029/2020GL088664>

- Finney, D., Marsham, J., Jackson, L., Kendon, E., Rowell, D., Boorman, P., et al. (2019). Implications of improved representation of convection for the East Africa water budget using a convection-permitting model. *Journal of Climate*, 32, 2109–2129. <https://doi.org/10.1175/JCLI-D-18-0387.1>
- Funk, C., Peterson, P., Landsfeld, M., Pedreros, D., Verdin, J., Shukla, S., et al. (2015). The climate hazards infrared precipitation with stations – A new environmental record for monitoring extremes. *Scientific Data*, 2. <https://doi.org/10.1038/sdata.2015.66>
- Gebrechorkos, S. H., Hülsmann, S., & Bernhofer, C. (2018). Evaluation of multiple climate data sources for managing environmental resources in East Africa. *Hydrology and Earth System Sciences*, 22, 4547–4564. <https://doi.org/10.5194/hess-22-4547-2018>
- Gelaro, R., McCarty, W., Suárez, M. J., Todling, R., Molod, A., Takacs, L., et al. (2017). The Modern-Era Retrospective Analysis for Research and Applications, Version 2 (MERRA-2). *Journal of Climate*, 30, 5419–5454. <https://doi.org/10.1175/JCLI-D-16-0758.1>
- Giannini, A., Lyon, B., Seager, R., & Vigaud, N. (2018). Dynamical and thermodynamic elements of modelled climate change at the East African margin of convection. *Geophysical Research Letters*, 45, 992–1000. <https://doi.org/10.1002/2017GL075486>
- Graham, R., O'Reilly, C., Otieno, G., Todd, M., & Todd, M. (2020). Causal pathways linking different flavours of ENSO with the Greater Horn of Africa short rains. *Atmospheric Science Letters*, 22, e1015. <https://doi.org/10.1002/asl.1015>
- Hartman, A. T. (2018). An analysis of the effects of temperatures and circulations on the strength of the low-level jet in the Turkana Channel in East Africa. *Theoretical and Applied Climatology*, 132, 1003–1017. <https://doi.org/10.1007/s00704-017-2121-x>
- Hastenrath, S., Polzin, D., & Mutai, C. (2007). Diagnosing the 2005 Drought in Equatorial East Africa. *Journal of Climate*, 20, 4628–4637. <https://doi.org/10.1175/JCLI4238.1>
- Hawkins, E., & Sutton, R. (2011). The potential to narrow uncertainty in projections of regional precipitation change. *Climate Dynamics*, 37, 407–418. <https://doi.org/10.1007/s00382-010-0810-6>
- Hirons, L., & Turner, A. (2018). The impact of Indian Ocean mean-state biases in climate models on the representation of the East African short rains. *Journal of Climate*, 31, 6611–6631. <https://doi.org/10.1175/JCLI-D-17-0804.1>
- Hoell, A. C., & Funk, C. (2014). Indo-Pacific sea surface temperature influences on failed consecutive rainy seasons over eastern Africa. *Climate Dynamics*, 43, 1645–1660. <https://doi.org/10.1007/s00382-013-1991-6>
- Hoell, A. C., Hoerling, M., Eischeid, J., Quan, X. W., Liebmann, B. (2017). Reconciling theories for human and natural attribution of recent East Africa drying. *Journal of Climate*, 30, 1939–1956. <https://doi.org/10.1175/JCLI-D-16-0558.1>
- Hua, W., Zhou, L., Nicholson, S. E., Chen, H., & Qin, M. (2019). Assessing reanalysis data for understanding rainfall climatology and variability over Central Equatorial Africa. *Climate Dynamics*, 53, 651–669. <https://doi.org/10.1007/s00382-018-04604-0>
- Jackson, L. S., Finney, D. L., Kendon, E. J., Marsham, J. H., Parker, D. J., Stratton, R. A., et al. (2020). The effect of explicit convection on couplings between rainfall, humidity, and ascent over Africa under climate change. *Journal of Climate*, 33, 8315–8337. <https://doi.org/10.1175/JCLI-D-19-0322.1>
- James, R., Washington, R., Abiodun, B., Kay, J., Mutemi, G. W., Senior, C., Pokam, W., et al. (2018). Evaluating climate models with an African lens. *Bulletin of the American Meteorological Society*, 99, 313–336. <https://doi.org/10.1175/BAMS-D-16-0090.1>
- Jaramillo, J., Muchugu, E., Vega, F. E., Davis, A., Borgemeister, C., & Chabi-Olaye, A. (2011). Some like it hot: The influence and implications of climate change on coffee berry borer (*Hypothenemus hampei*) and coffee production in East Africa. *PloS One*, 6, e24528. <https://doi.org/10.1371/journal.pone.0024528>
- Kaunda, C. S., Kimambo, C. Z., & Nielsen, T. K. (2012). Potential of small-scale hydropower for electricity generation in sub-Saharan Africa. *ISRN Renewable Energy*, 132606. <https://doi.org/10.5402/2012/132606>
- Kimani, M. W., B Hoedjes, J. C., & Su, Z. (2017). An assessment of satellite-derived rainfall products relative to ground observations over East Africa. *Remote Sensing*, 9, 430. <https://doi.org/10.3390/rs9050430>
- King, J. A., Engelstaedter, S., Washington, R., & Munday, C. (2021). Variability of the Turkana low-level jet in reanalysis and models: Implications for rainfall. *Journal of Geophysical Research Atmospheres*, 126, e2020JD034154. <https://doi.org/10.1029/2020JD034154>
- King, J. A., Washington, R., & Engelstaedter, S. (2020). Representation of the Indian Ocean walker circulation in climate models and links to Kenyan Rainfall. *International Journal of Climatology*, 41. <https://doi.org/10.1002/joc.6714>
- Kinuthia, J. H., & Asnani, G. C. (1982). A newly found jet in North Kenya (Turkana Channel). *Monthly Weather Review*, 110, 1722–1728. [https://doi.org/10.1175/1520-0493\(1982\)110<1722:ANFJIN>2.0.CO;2](https://doi.org/10.1175/1520-0493(1982)110<1722:ANFJIN>2.0.CO;2)
- Kociuba, G., & Power, S. B. (2015). Inability of CMIP5 models to simulate recent strengthening of the Walker Circulation: Implications for projections. *Journal of Climate*, 28, 20–35. <https://doi.org/10.1175/JCLI-D-13-00752.1>
- L'Heureux, M. L., Lee, S., & Lyon, B. (2013). Recent multidecadal strengthening of the Walker Circulation across the tropical Pacific. *Nature Climate Change*, 3, 571–576. <https://doi.org/10.1038/nclimate1840>
- Liebmann, B., Bladé, I., Funk, C., Allured, D., Quan, X., Hoerling, A., et al. (2017). Climatology and interannual variability of boreal spring wet season precipitation in the Eastern Horn of Africa and implications for its recent decline. *Journal of Climate*, 30, 3867–3886. <https://doi.org/10.1175/JCLI-D-16-0452.1>
- Liebmann, B., Hoerling, M. P., Funk, C., Bladé, I., Dole, R. M., Allured, D., et al. (2014). Understanding recent Eastern Horn of Africa rainfall variability and change. *Journal of Climate*, 27, 8630–8645. <https://doi.org/10.1175/JCLI-D-13-00714.1>
- Lyon, B. (2014). Seasonal drought in the Greater Horn of Africa and its recent increase during the March-May Long Rains. *Journal of Climate*, 27, 7953–7975. <https://doi.org/10.1175/JCLI-D-13-00459.1>
- MacLeod, D., Graham, R., O'Reilly, C., Otieno, G., Todd, M. (2020). Causal pathways linking different flavours of ENSO with the Greater Horn of Africa short rains. *Atmosphere Science Letters*, e1015. <https://doi.org/10.1002/asl.1015>
- Maidment, R., Allan, R. P., & Black, E. (2015). Recent observed and simulated changes in precipitation over Africa. *Geophysical Research Letters*, 42, 8155–8164. <https://doi.org/10.1002/2015GL065765>
- McKenna, S., Santoso, A., Gupta, A. S., Taschetto, A. S., & Cai, W. (2020). Indian Ocean Dipole in CMIP5 and CMIP6: Characteristics, biases, and links to ENSO. *Science Reports*, 10, 11500. <https://doi.org/10.1038/s41598-020-68268-9>
- McSweeney, C. F., Jones, R. G., Lee, R. W., & Rowell, D. P. (2015). Selecting CMIP5 GCMs for downscaling over multiple regions. *Climate Dynamics*, 44, 3237–3260. <https://doi.org/10.1007/s00382-014-2418-8>
- Mutai, C., Polzin, D., & Hastenrath, S. (2012). Diagnosing Kenya rainfall in boreal autumn: Further exploration. *Journal of Climate*, 25, 4323–4329. <https://doi.org/10.1175/JCLI-D-11-00414.1>
- Mutai, C., & Ward, M. N. (2000). East African Rainfall and the tropical circulation/convection on intraseasonal to interannual timescales. *Journal of Climate*, 13, 3915–3939.
- Naiman, Z., Goodman, P. J., Krasting, J. P., Malyshev, S. L., Russell, J. L., Stouffer, R. J., & Wittenberg, A. T. (2017). Impact of mountains on tropical circulation in two earth system models. *Journal of Climate*, 30, 4149–4163. <https://doi.org/10.1175/JCLI-D-16-0512.1>
- Nicholson, S. E. (2015). Long-term variability of the East African 'short rains' and its links to large-scale factors. *International Journal of Climatology*, 35, 3979–3990. <https://doi.org/10.1002/joc.4259>

- Nicholson, S. E. (2016). The Turkana low-level jet: Mean climatology and association with regional aridity. *International Journal of Climatology*, 36, 2598–2614. <https://doi.org/10.1002/joc.4515>
- Nicholson, S. E. (2017). Climate and climatic variability of rainfall over eastern Africa. *Review of Geophysics*, 55, 590–635. <https://doi.org/10.1002/2016RG000544>
- Ongoma, V., Chen, H., & Gao, C. (2019). Evaluation of CMIP5 twentieth century rainfall simulation over the equatorial East Africa. *Theoretical and Applied Climatology*, 135, 893–910. <https://doi.org/10.1007/s00704-018-2392-x>
- Onyango, E. A., Sahin, O., Awiti, A., Chu, C., & Mackey, B. (2016). An integrated risk and vulnerability assessment framework for climate change and malaria transmission in East Africa. *Malaria Journal*, 15, 551. <https://doi.org/10.1186/s12936-016-1600-3>
- Pfahl, S., O’Gorman, P., & Fischer, E. (2017). Understanding the regional pattern of projected future changes in extreme precipitation. *Nature Climate Change*, 7, 423–427. <https://doi.org/10.1038/nclimate3287>
- Philip, S., Kew, S. F., van Oldenborgh, G. J., Otto, F., O’Keefe, S., Haustein, K., et al. (2018). Attribution analysis of the Ethiopian Drought of 2015. *Journal of Climate*, 31, 2465–2486. <https://doi.org/10.1175/JCLI-D-17-0274.1>
- Rowell, D. P., Booth, B. B., Nicholson, S. E., & Good, P. (2015). Reconciling past and future rainfall trends over East Africa. *Journal of Climate*, 28, 9768–9788. <https://doi.org/10.1175/JCLI-D-15-0140.1>
- Rowell, D. P., & Chadwick, R. (2018). Causes of the uncertainty in projections of tropical terrestrial rainfall change: East Africa. *Journal of Climate*, 31, 5977–5995. <https://doi.org/10.1175/JCLI-D-17-0830.1>
- Rowell, D. P., Senior, C. A., Vellinga, M., & Graham, R. J. (2016). Can climate projection uncertainty be constrained over Africa using metrics of contemporary performance? *Climatic Change*, 134, 621–633. <https://doi.org/10.1007/s10584-015-1554-4>
- Salami, A., Kamara, A. B., & Brixiova, Z. (2010). Smallholder agriculture in East Africa: Trends, constraints, and opportunities. *African Development Bank Working Papers Series No. (Vol. 105)*. African Development Bank.
- Sanford, T., Frumhoff, P. C., Luers, A., & Gullett, J. (2014). The climate policy narrative for a dangerously warming world. *Nature Climate Change*, 4, 164–166. <https://doi.org/10.1038/nclimate2148>
- Senior, C. A. M., Graham, R. J., Vellinga, M., & Graham, R. J. (2016). Can climate projection uncertainty be constrained over Africa using metrics of contemporary performance? *Climatic Change*, 134, 621–633. <https://doi.org/10.1007/s10584-015-1554-4>
- Stratton, R. A., Senior, C. A., Vosper, S. B., Folwell, S. S., Boutle, I. A., Earnshaw, P. D., et al. (2018). A Pan-African convection-permitting regional climate simulation with the met office unified model: CP4-Africa. *Journal of Climate*, 31, 3485–3508. <https://doi.org/10.1175/JCLI-D-17-0503.1>
- Taylor, K. E., Stouffer, R. J., & Meehl, G. A. (2012). An overview of CMIP5 and the experiment design. *Bulletin of the American Meteorological Society*, 93, 485–498. <https://doi.org/10.1175/BAMS-D-11-00094.1>
- Thalheimer, L., & Webersik, C. (2020). Climate change, conflicts and migration. In T. Krieger, T. Krieger, T. Krieger, D. Panke, D. Panke, D. Panke, & M. Pregering, M. Pregering, M. Pregering (Eds.), *Environmental conflicts, migration and governance* (pp. 59–82). Bristol University Press. <https://doi.org/10.46692/9781529202175.004>
- Tierney, J., Ummenhofer, C. C., & de Menocal, P. B. (2015). Past and future rainfall in the Horn of Africa. *Science Advances*, 1, e1500682. <https://doi.org/10.1126/sciadv.1500682>
- Torralba, V., Doblas-Reyes, F. J., & Gonzalez-Reviriego, N. (2017). Uncertainty in recent near-surface wind speed trends: A global reanalysis intercomparison. *Environmental Research Letters*, 12, 114019. <https://doi.org/10.1088/1748-9326/aa8a58>
- Vellinga, M., & Milton, S. F. (2018). Drivers of interannual variability of the East African long rains. *Quarterly Journal of the Royal Meteorological Society*, 144, 861–876. <https://doi.org/10.1002/qj.3263>
- Verschuren, D., Laird, K. R., & Cumming, B. F. (2000). Rainfall and drought in equatorial east Africa during the past 1,100 years. *Nature*, 403, 410–414. <https://doi.org/10.1038/35000179>
- Vigaud, N., Lyon, B., & Giannini, A. (2017). Sub-seasonal teleconnections between convection over the Indian Ocean, the East African long rains and tropical Pacific surface temperatures. *International Journal of Climatology*, 37, 1167–1180. <https://doi.org/10.1002/joc.4765>
- Wainwright, C. M., Marsham, J. H., Keane, R. J., Rowell, D. P., Finney, D. L., Black, E., & Allan, R. P. (2019). ‘Eastern African Paradox’ rainfall decline due to shorter not less intense Short Rains. *NPJ Climate and Atmospheric Science*, 2. <https://doi.org/10.1038/s41612-019-0091-7>
- Walker, D. P., Marsham, J. H., Birch, C. E., Scaife, A. A., & Finney, D. L. (2020). Common mechanism for interannual and decadal variability in the East African Long Rains. *Geophysical Research Letters*, 47, e2020GL089182. <https://doi.org/10.1029/2020GL089182>
- Washington, R., James, R., Pearce, H., Pokam, W. M., & Moufouma-Okia, W. (2013). Congo Basin rainfall climatology: Can we believe the climate models? *Philosophical Transactions of the Royal Society B*, 368, 20120296. <https://doi.org/10.1098/rstb.2012.0296>
- Williams, A. P., & Funk, C. (2011). A westward extension of the warm pool leads to a westward extension of the Walker circulation, drying eastern Africa. *Climate Dynamics*, 37, 2417–2435. <https://doi.org/10.1007/s00382-010-0984-y>
- Yang, K., Cai, W., Huang, G., Wang, G., Ng, B., & Li, S. (2020). Oceanic processes in ocean temperature products key to a realistic presentation of positive Indian Ocean dipole nonlinearity. *Geophysical Research Letters*, 47, e2020GL089396. <https://doi.org/10.1029/2020GL089396>
- Yang, W., Seager, R., Cane, M. A., & Lyon, B. (2015). The rainfall annual cycle bias over East Africa in CMIP5 coupled climate models. *Journal of Climate*, 28, 9789–9802. <https://doi.org/10.1175/JCLI-D-15-0323.1>
- Zaitchik, B. (2017). Madden-Julian Oscillation impacts on tropical African precipitation. *Atmospheric Research*, 184, 88–102. <https://doi.org/10.1016/j.atmosres.2016.10.002>
- Zhao, S., & Cook, K. H. (2021). Influence of walker circulations on East African rainfall. *Climate Dynamics*, 56, 2127–2147. <https://doi.org/10.1007/s00382-020-05579-7>